Geometric Stability of Reciprocal Structures

Martin Steinmetz[1]; Luca Sgambi[2]; and Pierre Latteur[3]

Abstract: Reciprocal structures exhibit complex geometries with an architectural and structural appearance that lacks a clear hierarchy. This absence of hierarchy makes the design of their connections particularly challenging, especially when aiming to prevent local and global geometric instabilities, such as rigid beam rotations around their longitudinal axes, among other issues. As a result, there is significant uncertainty and a general lack of confidence among designers toward reciprocal structures. This is further exacerbated by the absence of well-defined design guidelines for connections and a universal method for assessing their geometric stability. Consequently, most reciprocal structures built worldwide are limited to either elementary modules or simplified geometries, or rely on completely fixed or welded connections, compromising the essence of reciprocity and aligning them more closely with the principles of gridshells. This paper sheds light on how reciprocal structures should be designed in terms of global geometry, connections, and supports, and it compares the effectiveness of five methods for evaluating their geometric stability. **DOI: 10.1061/JSENDH.STENG-15466.** *© 2025 American Society of Civil Engineers.*

Author keywords: Reciprocal structures; Geometric stability assessment; Stability rules; Instability; Connections; Supports.

Introduction

Definitions

A reciprocal structure (RS) consists of one or several simple modules, each comprising at least three beams [Fig. 1(a)]. An infinite number of possible assemblies of such simple modules allows for generating geometries of virtually unlimited variety (Fig. 1). The RS offers a dual advantage: On one hand, it presents an unusual and striking architectural appearance; on the other hand, it enables the spanning of large distances through the superposition of small elements. For this latter reason, RSs are typically constructed using timber beams, as wood is naturally limited in length. RSs follow three fundamental design rules (Latteur et al. 2021):

- Each beam supports at least one other beam.
- Each beam end is supported either on another beam or a support.
- Each support carries only a single beam.

RSs should not be confused with gridshells, which are structures composed of crossed grids of beams, usually long, thin, flexible, and interconnected, whose overall rigidity comes from the membrane effect, and rigid or partially rigid nodes.

In RSs, beam types can be defined according to the number of supports and connections. Fig. 2 illustrates the most common types, the only ones considered in this paper.

This paper also distinguishes between the following types of reciprocal structures:

- Plane reciprocal structures subjected to out-of-plane loading, referred to as RS^{2D}, in which the beam axes lie within the same plane [Fig. 3(a)].
- Spatial reciprocal structures, referred to as RS^{3D} [Fig. 3(b)]. In RS^{3D}, the supported beam may be suspended from the supporting beam.

In both cases, the connection is characterized by an eccentricity e as indicated in Fig. 3. Whether dealing with RS^{2D} or RS^{3D}, a distinction is made (Fig. 3) between

- a reciprocal structure composed of a single module (SM RS^{2D} or SM RS^{3D}), and composed only of beams type 1; and
- a reciprocal structure composed of multiple modules (MM RS^{2D} or MM RS^{3D}).

Objectives

This paper aims to critically present various types of supports and connections proposed in the literature and compares five methods for verifying the geometric stability of RSs. This article does not consider instabilities due to local or global buckling.

During the design of a reciprocal structure, the choice of supports and connections, particularly the types of constraints they introduce, must be carefully considered for the following reasons:

- They can be the source of local instabilities, such as rotating rigid beams around their longitudinal axis.
- The actual behavior of supports and connections is often challenging to model numerically with sufficient accuracy (Rizzuto 2018), which may result in the imprecise calculation of internal forces within the beams (Franke et al. 2017), especially in RS^{3D}.
- The connections determine the eccentricity between beams, which influences the overall shape and curvature of the structure (Baverel 2000). Modifying one or more connections can therefore affect the global geometry, which must then be generated iteratively (Parigi and Kirkegaard 2014b).
- Supports and connections should allow for straightforward construction and facilitate the mutual assembly of the beams, while also maintaining the designed geometry (Anastas et al. 2016).

[1]Ph.D. Student, Louvain Research Institute for Landscape, Architecture, Built Environment, UCLouvain, Louvain-la-Neuve 1348, Belgium (corresponding author). ORCID: https://orcid.org/0000-0001-6378-5368. Email: martin.steinmetz@uclouvain.be

[2]Professor, Louvain Research Institute for Landscape, Architecture, Built Environment, UCLouvain, Louvain-la-Neuve 1348, Belgium. Email: luca.sgambi@uclouvain.be

[3]Professor, Institute of Mechanics, Materials and Civil Engineering, UCLouvain, Louvain-la-Neuve 1348, Belgium. Email: pierre.latteur@uclouvain.be

Note. This manuscript was submitted on May 12, 2025; approved on August 6, 2025; published online on December 26, 2025. Discussion period open until May 26, 2026; separate discussions must be submitted for individual papers. This paper is part of the ***Journal of Structural Engineering***, © ASCE, ISSN 0733-9445.

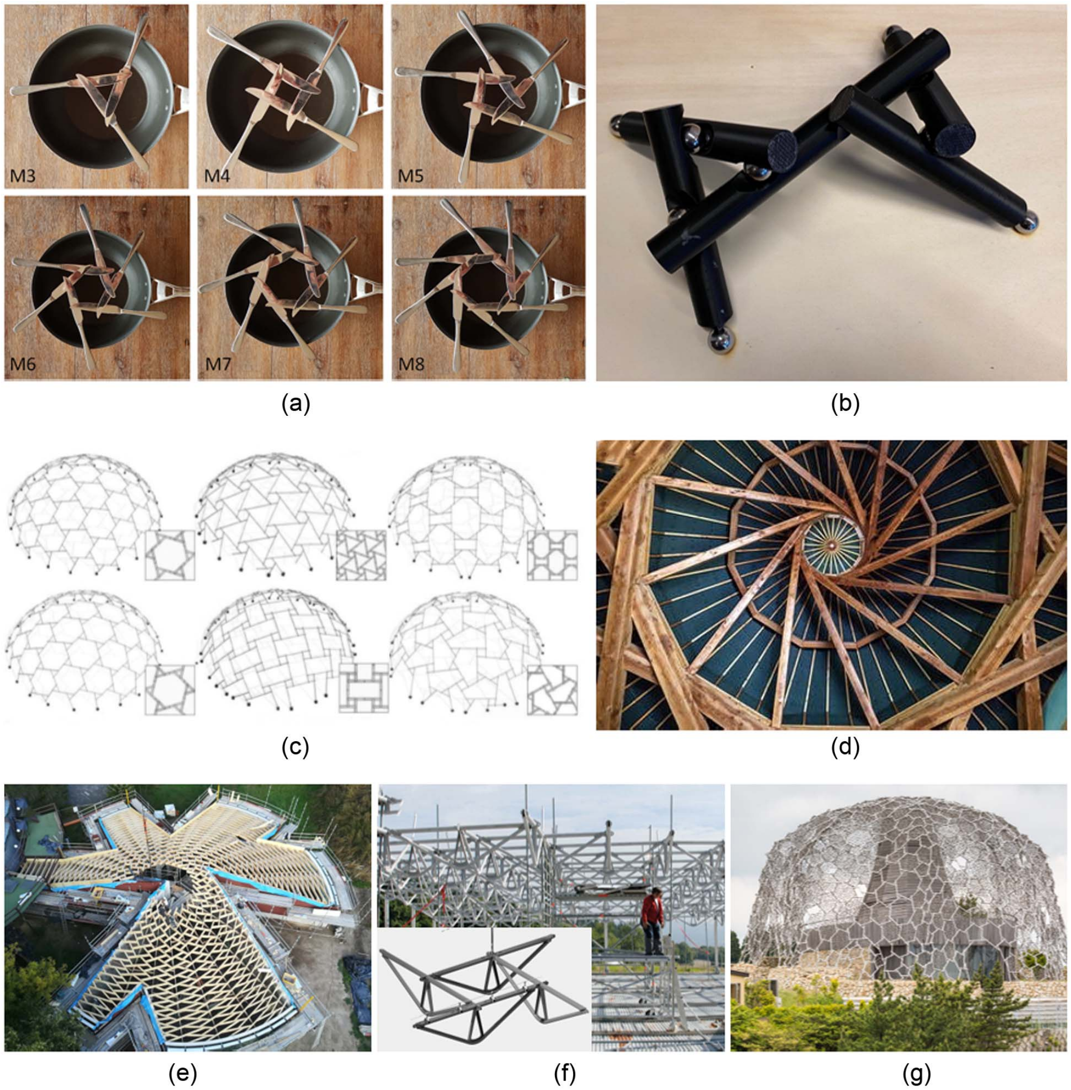

Fig. 1. (a) Simple modules of the reciprocal structures (P. Latteur, J. Geno, and M. Vandamme, "Design rules for timber log reciprocal floors, based on mass optimization under stiffness constraint." *International Journal of Space Structures* 36 (3), © 2021 by SAGE, reprinted by permission of SAGE Publications, Ltd.); (b) 3D printing reciprocal structure (image by authors); (c) different dome patterns (reprinted with permission from Song et al. 2013); (d) roof of the Seiwa Exhibition Hall (Japan) [connection details in Fig. 8(b)] (image courtesy of Olga Popovic Larsen); (e) roof of the Frans Masereel Pavilion (Belgium) by TimberFraming [connection details in Fig. 9(d)] (image courtesy of Kasimir Ketele); (f) archaeological site in Bibracte (France) [connection details in Fig. 11(c)] (image courtesy of Louise Daquin); and (g) roof of the Rokko Shidare Observatory (Japan) [connection details in Fig. 11(a)] (image by authors).

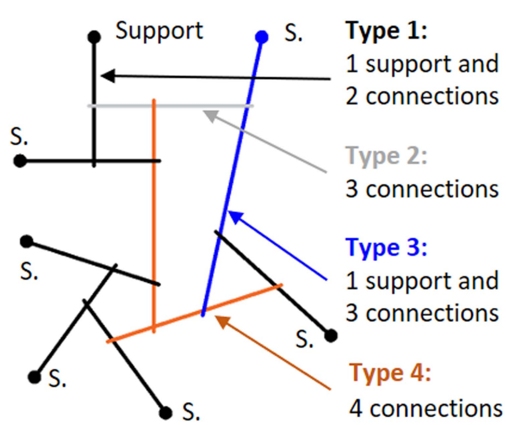

Fig. 2. Beam types in a schematically represented RS. Beam ends with circles are associated with supports (S.).

- Translational constraints at the supports may generate horizontal reaction forces that are sometimes incompatible with the project requirements, even though such constraints may enhance structural stability.

The following section reviews different types of supports and connections, both in built structures and laboratory prototypes. Then, five methods are compared for evaluating the geometric stability of RS^{2D} and RS^{3D}, including methods explicitly developed for RSs and those that can be adapted to them. The first method is based on the structure's stiffness matrix and is thus dependent on cross-section and material properties. The remaining four methods assume infinitely rigid beams and require fewer computational resources. Given that the geometric design of an RS is often iterative (Douthe and Baverel 2009), these methods are particularly valuable for accelerating the design process.

The support and connection models considered in this paper are illustrated in Fig. 4. Each may have six degrees of freedom (DoFs),

J. Struct. Eng., 2026, 152(3): 04025288

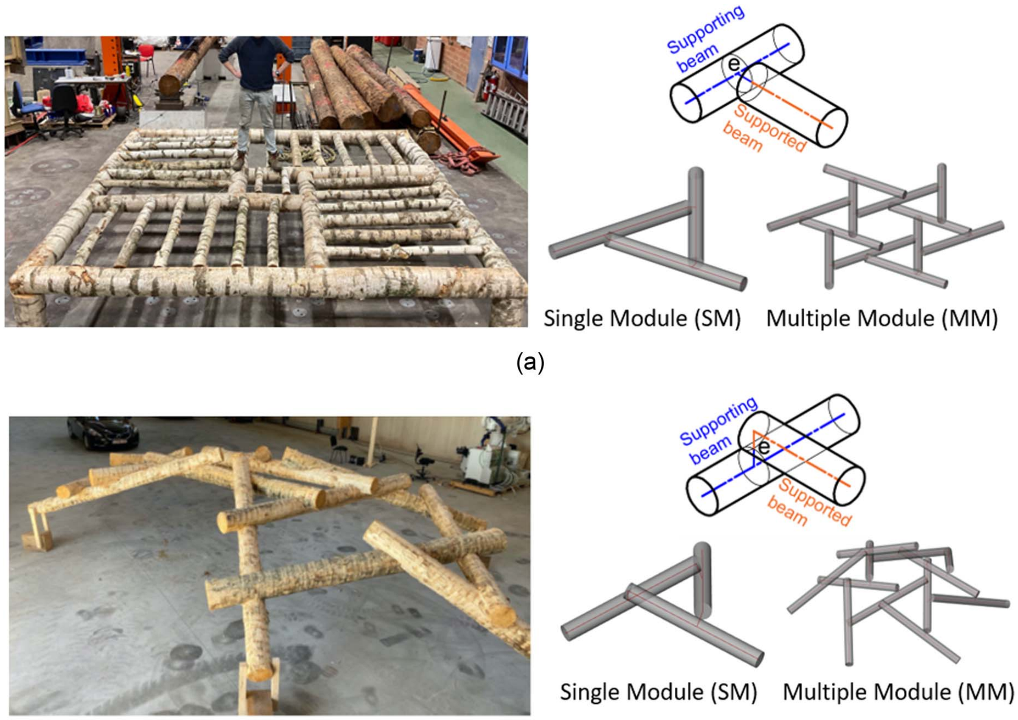

Fig. 3. (a) Plane reciprocal structures, with an RS^{2D} log floor made by the authors (reprinted from *Engineering Structures*, Vol. 297, M. Steinmetz, P. Latteur, and L. Sgambi, "Optimal log floor patterns," 116970, © 2023, with permission from Elsevier); and (b) spatial reciprocal structures, an RS^{3D} constructed by the authors (image by authors).

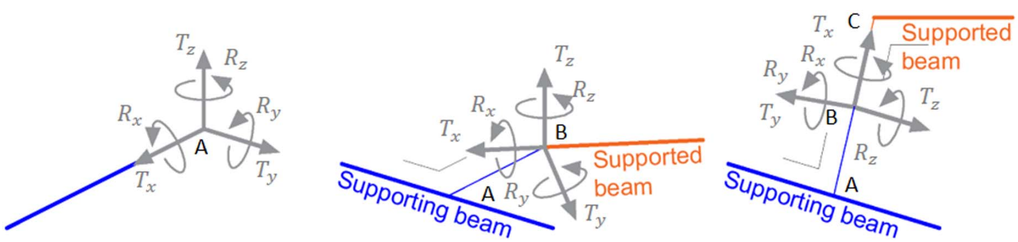

Fig. 4. Six free, semirigid, or fixed DoFs, presented by arrows when fixed: (a) support; (b) RS^{2D} connection placed at point B; and (c) RS^{3D} connection placed at point B.

which can be free, semirigid, or fixed. The fixed DoFs are indicated with arrows (T_x, T_y, T_z, R_x, R_y, and R_z). In particular, when only the three translational DoFs are fixed (free R_x, R_y, and R_z), the support or connection is called "hinged." An RS_{HINGED} has only hinged supports and connections. Furthermore, the beam thickness's eccentricity is modeled using a fictitious element AB for RS^{2D} [Fig. 4(b)] or two fictitious elements AB and BC for RS^{3D} [Fig. 4(c)], with clamped connections at A and C. If any presented supports or connections deviate from these assumptions, their modeling approach will be explicitly specified.

State of the Art Regarding Supports and Connections of RS

Supports

Fig. 5 presents examples of supports used in laboratory-tested reciprocal structures (RS) or described in the scientific literature:

- Fig. 5(a): Two support solutions for an RS^{3D} built with bamboo canes are proposed by Godina Rodriguez (2019). In the first case, the bamboo beam is placed on the ground, and the support is modeled as restraining only vertical translation. The second solution incorporates cables connecting the three supports, thereby limiting lateral displacements [zoom of Fig. 5(a)]. These cables are not considered infinitely rigid, and are thus modeled as semirigid horizontal translational DoF, with stiffness values derived from their mechanical properties.
- Fig. 5(b): This refers to an experimental metallic structure in which the support tubes were cut obliquely and rested directly on the ground (Rizzuto 2018). These supports are modeled by fixing only the vertical translation, or by adding semirigid horizontal translational DoFs to account for friction. The stiffness of these semirigidities is determined based on measured displacements during testing.
- Fig. 5(c): For this RS^{2D} built with steel tubes, Steinmetz et al. (2024) proposed a support that fixes rotation about the tube's axis (R_x) using a sufficiently wide plate welded under the tube

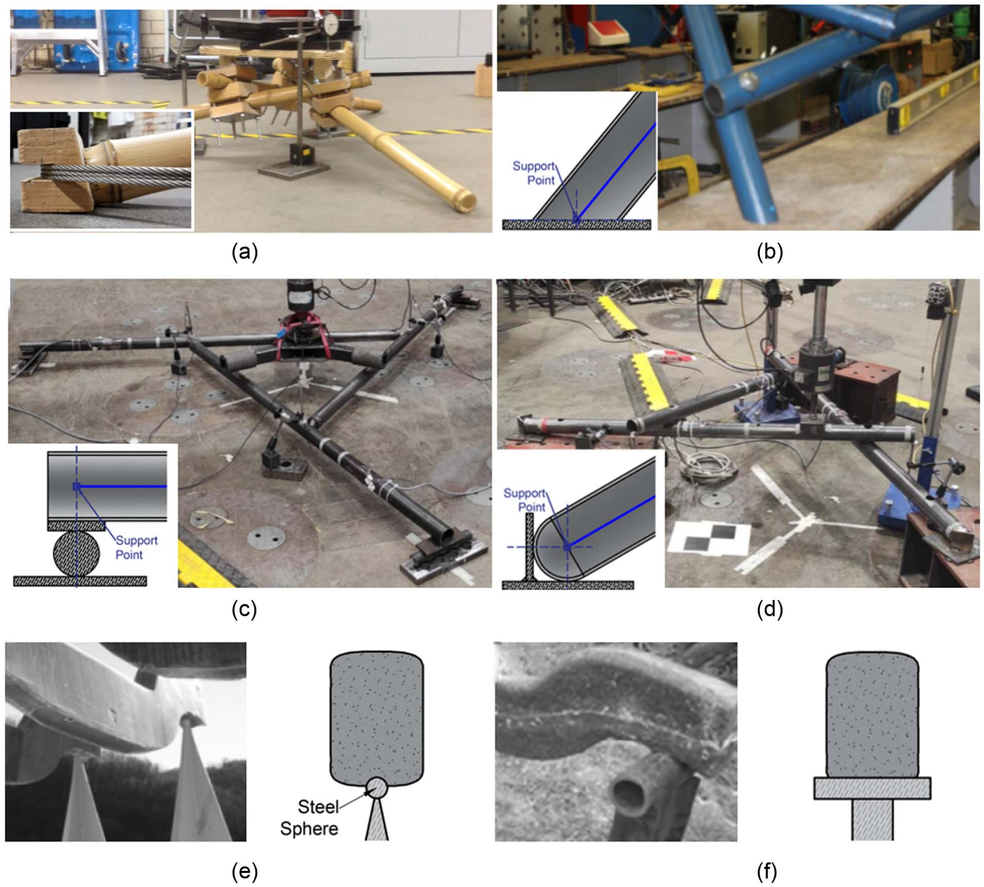

Fig. 5. Various supports for experimental RS: (a) support for bamboo RS (images courtesy of Martha Godina Rodríguez); (b) circular tube laid on a horizontal surface (image courtesy of Joseph Rizzuto); (c) tube with welded plate, laid on support roll (image by authors); (d) circular tube with a hemisphere welded at the end (image by authors); (e) concrete beam on fixed sphere; and (f) concrete beam on tube. [Images (e and f) courtesy of Attilio Pizzigoni.]

and resting on a rolling metal cylinder. Vertical translation (T_z) is fixed. Lateral translation perpendicular to the tube's axis (T_y) is not mechanically restrained, but because the loading is purely vertical, it is modeled as fixed.

- Fig. 5(d): For this RS^{3D}, also made of steel tubes, the same authors (Steinmetz et al. 2024) proposed to weld a hemisphere at the tube's end, which fits into a corner bracket. This allows the support to be modeled as a hinge located along the tube axis, at the center of the hemisphere. This solution is valid as long as there is no tension in the tube and horizontal thrusts are either permitted at the supports or absent.
- Figs. 5(e and f): For an RS^{2D}, built with fiber-reinforced concrete, Pizzigoni (2009) propose two types of supports: The beams are placed on fixed metal spheres [Fig. 5(e)] or metal tubes [Fig. 5(f)]. In the first case, the support is modeled as a hinge. Only the rotational DoF about the tube axis is left free in the second case.

Fig. 6 pertains to the supports of several existing timber structures, as follows:

- Fig. 6(a): The squared timber beam is inserted into a tenon and rests on a flat surface (Larsen 2008). All three translational DoFs are fixed in this configuration. The rotation about the beam's axis is prevented by secondary beams resting atop the reciprocal structure.
- Fig. 6(b): Logs are secured at the supports using ropes, effectively fixing all three translational DoFs (Wrench 2015).
- Fig. 6(c): For the supports of the pavilion shown in Fig. 1(e), the timber beams are laterally restrained by four through-rod and a steel beam shoe anchored into the substructure. In this case, all three translational DoFs are fixed. However, for specific supports where horizontal reaction forces were deemed unacceptable for the substructure, the holes in the brackets were made oblong to release translation along the beam axis (T_x) (M. Guillaume, personal communication, April 2025).

Fig. 7 illustrates other possible solutions proposed by the authors, as follows, either for timber RS or for steel RS:

- Fig. 7(a): A variant of the solution in Fig. 6(c), applied to RS^{3D} structures in timber.
- Fig. 7(b): The solutions shown in Figs. 6(c) and 7(a) also apply to round timber, provided the beam is locally machined into a rectangular section at the support area.
- Figs. 7(c and d): Supports for RS^{2D} and RS^{3D} using metal tubes. A metal plate is welded locally beneath the tube, fixing rotation (R_x) about the tube axis. The fixed DoFs are T_x, T_y, T_z, and R_x. By using oblong holes, the translational DoF along the beam axis can be released, thereby avoiding horizontal reaction forces.

Connections

Connections for Timber RSs

The connections must account for the variable mechanical properties of timber that depend on the orientation of the fibers, dimensional changes due to moisture, and potentially irregular geometry in the case of logs. A distinction is made between wood–wood

J. Struct. Eng., 2026, 152(3): 04025288

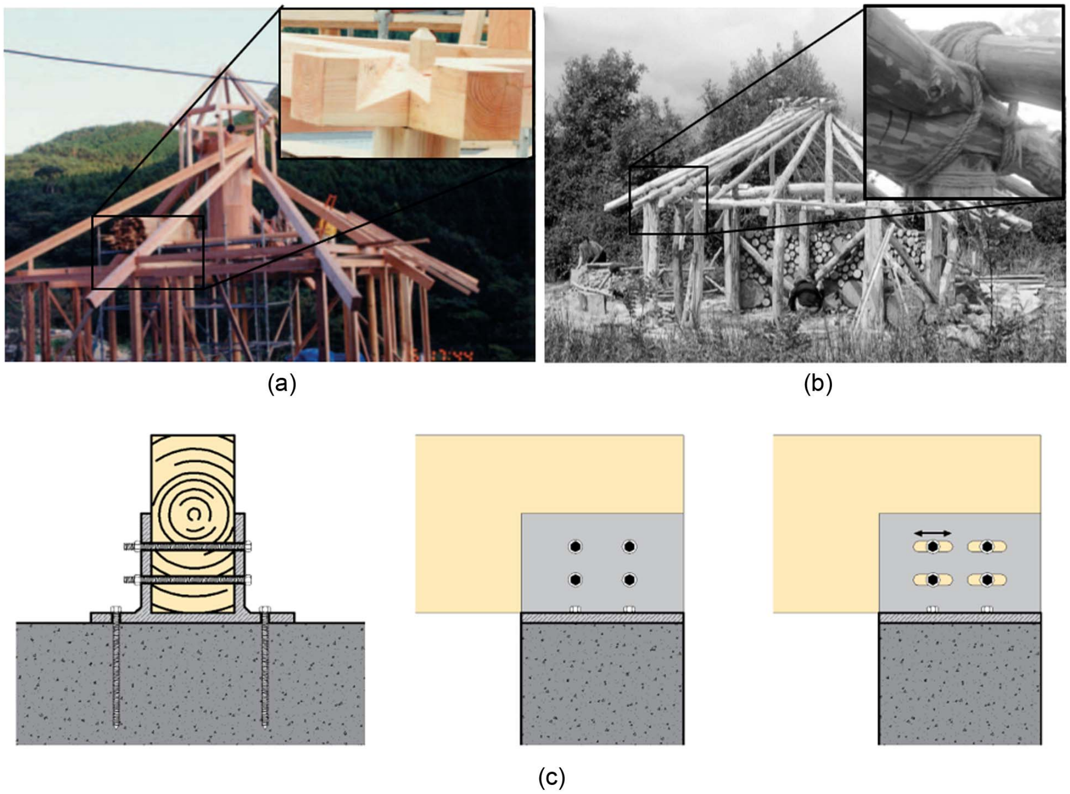

Fig. 6. Different supports of constructed RS: (a) wood–wood support for the roof of the New Farmhouse (Japan) (Image courtesy of Olga Popovic Larsen); (b) log support with ropes (reprinted with permission from Wrench 2015); and (c) Frans Masereel Pavilion support [Fig. 1(e)].

connections (Fig. 8) and connections incorporating fastening elements (Fig. 9).

A wood–wood connection is achieved by cutting the supporting and/or supported beams locally to create contact surfaces. These cuts may be carried out manually or with various tools, such as a robotic arm equipped with a cutting tool [Figs. 8(a and b)] (Geno et al. 2022; Larsson et al. 2019; Vestartas et al. 2021; Steinmetz et al. 2023).

Gustafsson (2016) modeled and experimentally tested a $5 \times 5\ \mathrm{m}^2$ RS^{2D} composed of squared timber with notched half-lap connections [Fig. 8(c)]. At the boundaries, the beam ends rest on trestles and are modeled as hinged supports. The connection is modeled with six semirigid DoFs, with stiffness values determined using the method proposed by Descamps and Guerlement (2009), as follows: For each movement (translation or rotation) of the supported beam, the pressure zones generated on the contact surfaces are converted into equivalent stiffness values based on the mechanical properties of the timber, neglecting friction. For small loads, the measured displacement was approximately three times greater than the calculated one, and the failure load was nearly 30% lower than the estimated value, exhibiting a brittle failure mode. These results highlight the difficulty of accurately modeling such connections based solely on contact surfaces. This type of connection can also generate RS^{3D} structures if the notches do not precisely halve the beam height, thus creating the necessary eccentricity, as proposed by Anastas et al. (2016).

The strength of wood–wood connections is improved when multiple faces are in contact; however, this makes stress transfer and modeling uncertain. In addition, it is difficult to predict which faces will be in contact due to machining tolerances, hygrometric variations, applied loads, and global structural deformation, all of which may vary (Geno et al. 2022). To limit these uncertainties, the connection geometry, shown in Fig. 8(a) and described by Geno et al. (2022), ensures that the contact planes are maintained despite dimensional variations, as the central area is not a contact surface [Fig. 8(a)]. The MM RS^{3D} structure made of logs, presented in Fig. 3(b), was constructed based on this type of connection (Geno et al. 2022). Its design was based on an idealized connection model, in which the fixed DoFs are the three translational movements (locked only in abutment) and the rotation around the eccentricity axis. This rotation mobilizes the four oblique contact surfaces in compression. This modeling choice aimed to ensure safety rather than accurately represent the structural behavior.

Vestartas et al. (2021) presented an RS^{3D} composed of logs assembled with a cut similar to that shown in Fig. 8(a), modeled by an element with six semirigid DoFs connecting the beam axes. The stiffness values are determined experimentally, as proposed by the same authors for a wood–wood connection between engineered timber boards (Nguyen et al. 2019). The numerical results are promising but have yet to be experimentally validated.

Many other types of joints between timber beams use screws, rods, connecting metal pieces, rope, adhesive, and so on (Bergis and Rycke 2019; Castriotto et al. 2022; Corio et al. 2017; Gustafsson 2016; Kohlhammer et al. 2017; Parigi and Kirkegaard 2014a; Godina Rodriguez 2019). Among these solutions, four are schematically represented in Fig. 9, explained as follows:

- Fig. 9(a): Godina Rodriguez (2019) developed a connection between two bamboo canes using three timber blocks, with computer numerical control (CNC) cut to match the curvature of the canes and ensure their respective orientations. These blocks are rigidly fixed using four steel rods. Steel plates are added on either side of the assembly to optimize the transfer of forces between the rods and the timber blocks. A neoprene membrane is placed at the bamboo and timber interface to distribute compressive stresses. Despite the neoprene, this connector is modeled as

J. Struct. Eng., 2026, 152(3): 04025288

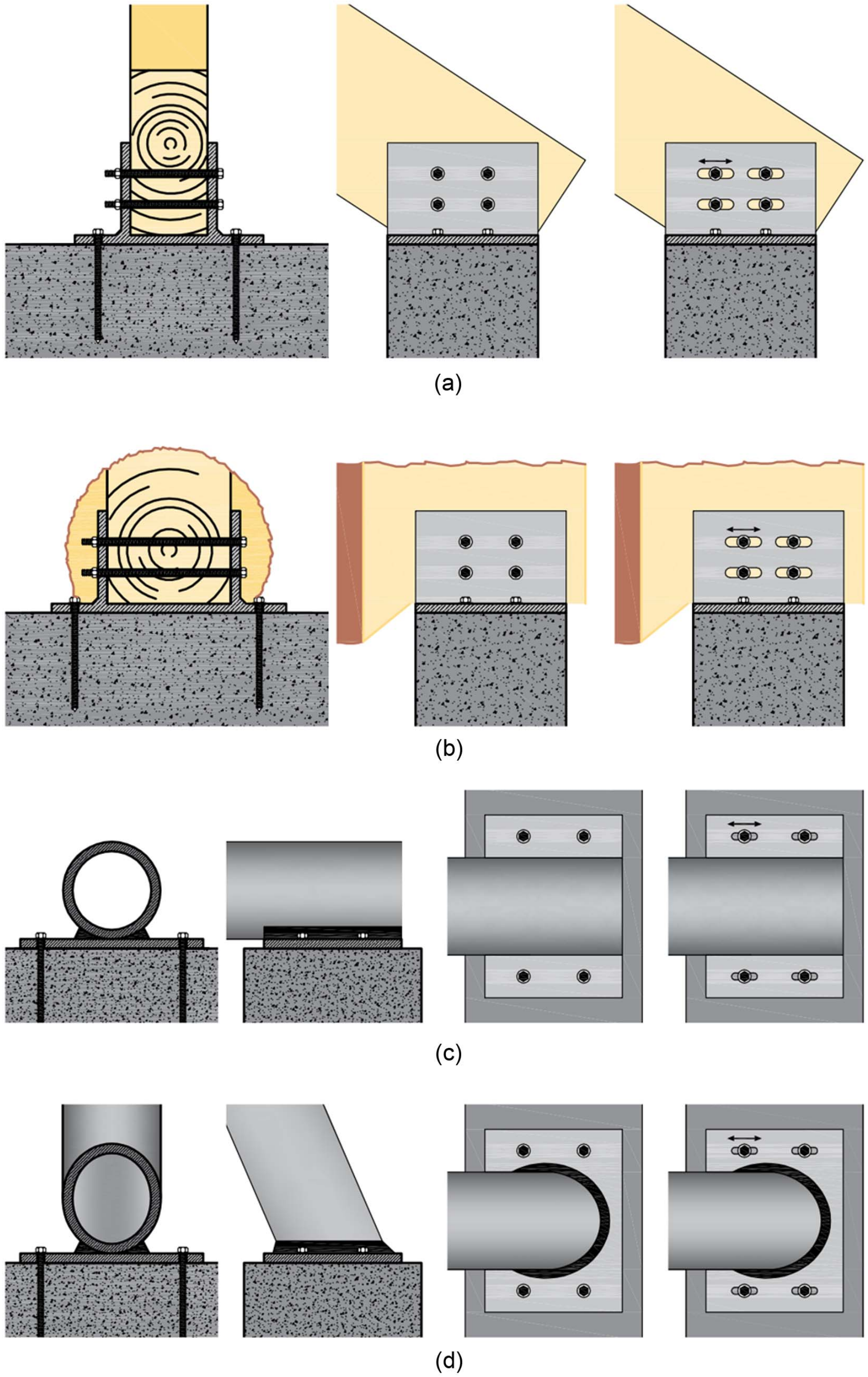

Fig. 7. Various RS supports proposed by the authors: (a) squared timber beams support for RS^{3D} with or without oblong holes; (b) round timber support; (c) support for RS^{2D} with welded tube to fixed plate; and (d) support for RS^{3D} with welded tube to fixed plate.

a rigid arm AB. The displacements provided by the numerical model are consistent with experimental measurements on an SM RS^{3D} with three canes for the two types of supports presented in Fig. 5(a). However, for an MM RS^{3D} structure composed of two single modules of three beams, geometrically similar to the RS shown in Fig. 1(b), the numerical model yields stiffer results than observed experimentally. The authors also highlight that the challenges of these tests cause imprecision: unknown precise mechanical properties of the bamboo and inaccuracies between the tested and the numerical geometry.

- Fig. 9(b): Kohlhammer et al. (2017) proposed a model for a connection between two squared beams glued laterally. To represent the local semirigid behavior of the bonded area, the glued assembly is modeled with three small beams, AB, BC, and CD, rigidly connected, but accounting for the glued areas and the timber properties perpendicular to the grain for beams AB and CD, and for the adhesive properties in beam BC (whose length is exaggerated in the drawing). This modeling captures the semirigid behavior of the connection but has not been experimentally validated.

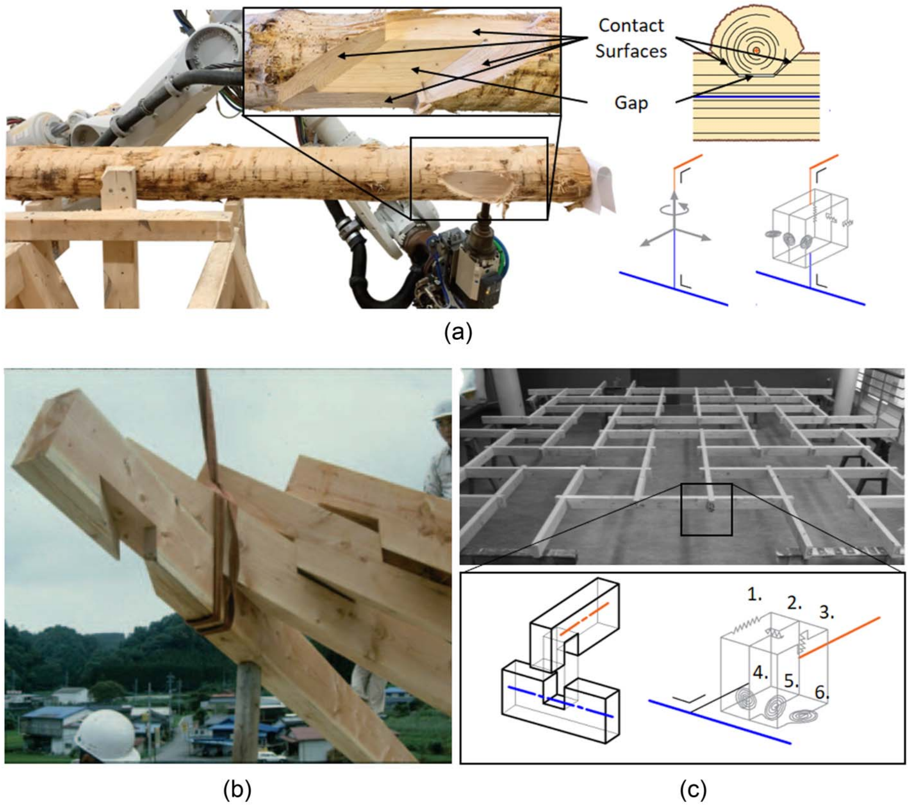

Fig. 8. Wood–wood connection: (a) log-to-log connection assembly diagram and models (reprinted from *Automation in Construction*, Vol. 138, J. Geno, J. Goosse, S. Van Nimwegen, and P. Latteur, "Parametric design and robotic fabrication of whole timber reciprocal structures." 104198, © 2022, with permission from Elsevier); (b) Bunraka Theatre (Japan) connection (image courtesy of Olga Popovic Larsen); and (c) RS^{2D} half-lap connection, assembly diagram and modeling with an element of six semirigid DoFs with uncoupled linear stiffness: 1. Longitudinal, 2. Transversal, 3. Lateral, 4. Torsional, 5. In transverse bending, and 6. In lateral bending. (reprinted with permission of Gustafsson 2016).

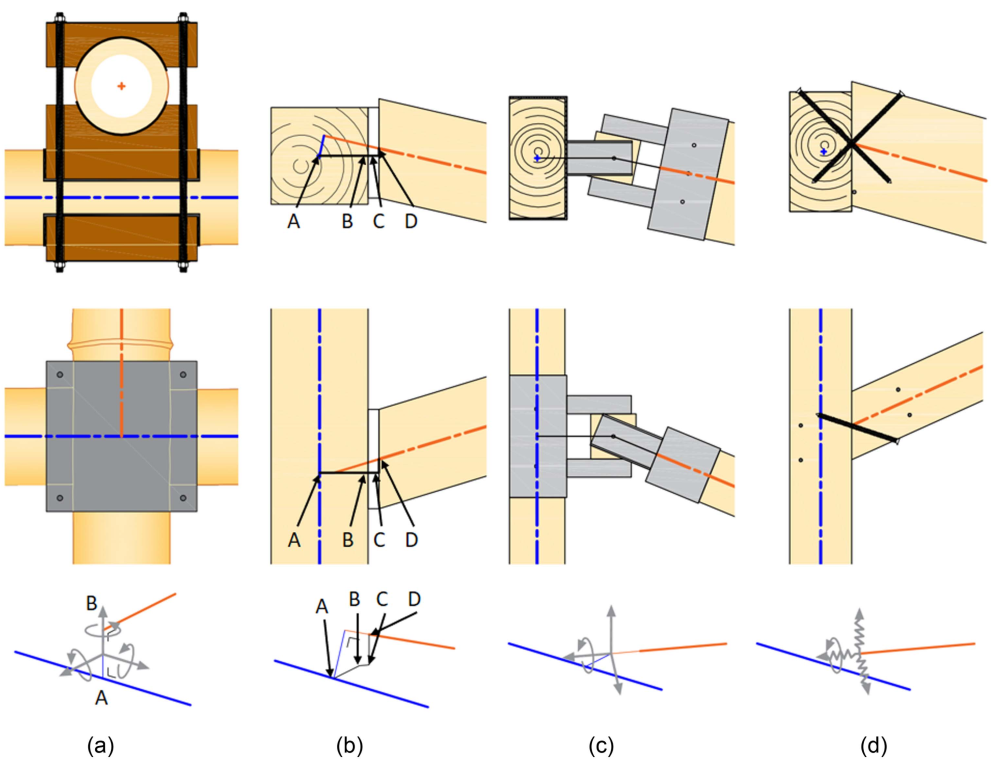

Fig. 9. Connection examples with section, top views, and modeling: (a) connection between two bamboo canes; (b) lateral glued connection; (c) lateral U-joint; and (d) Masureel center screwed connection [Fig. 1(e)].

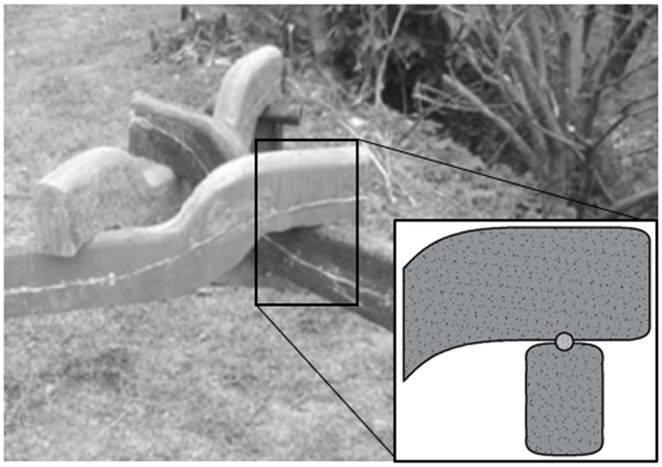

Fig. 10. SM RS^{2D} with three fiber concrete beams with connection detailing. (Image courtesy of Attilio Pizzigoni.)

- Fig. 9(c): Corio et al. (2017) presented a connection between two squared timber beams with a U-joint for RS^{3D} structures, although it has not been experimentally verified. This type of joint allows two rotational DoFs at the center of the timber block. Only the rotation around the eccentricity axis is fixed. However, this connection would yield when subjected to excessive torsion from the supported beam generated, for example, by eccentric loads.
- Fig. 9(d): For the Masereel Centre in Belgium [Fig. 1(e)], the chosen connection consists of five screws and is modeled with the three translational DoFs considered semirigid. As the beams are subsequently covered with timber panels, the rotational DoF around the axis of the carried beam is assumed to be fixed. Some highly loaded connections are reinforced with steel plates or glued dowels to increase their strength (M. Guillaume, personal communication, April 2025).

Connection for Concrete RSs

To the authors' knowledge, there is only one reference concerning RSs made of concrete, which describes an RS^{2D} prototype (Fig. 10) (Garavaglia1a et al. 2013; Pizzigoni 2009). The fiber-reinforced concrete beams are connected using a steel sphere at the interface. The sphere maintains the same contact point even after beam rotation due to bending. Numerical results obtained using a solid finite element model demonstrate good agreement with experimental measurements under static loading conditions. The supports are shown in Figs. 5(e and f). The connection can be modeled as a hinge in a beam-based model, provided the loading does not cause separation between the beams.

Connections for Metal RSs

Two examples of built metal structures with a reciprocal geometry are shown in Figs. 1(f and g), although such structures remain extremely rare. Due to its ease of welding, steel is generally preferred for gridshells. A few prototypes of RS^{3D} in metal have been tested in laboratories and are typically made of circular tubes, as their constant eccentricity, regardless of orientation, simplifies connections. Fig. 11 presents examples of connection solutions discussed in the literature or proposed by the authors, and summarized as follows:

- Fig. 11(a): Welded connection (Popovic Larsen 2014): This solution is used to join the tubes of the main structure of the Mount Rokko-Shidare Observatory, shown in Fig. 1(g). It can be modeled with all six DoFs fixed by the welds. However, this connection complicates the construction process, as the welds on curved surfaces are challenging to execute, and each tube must be accurately positioned to maintain the final geometry (Goto et al. 2011). Moreover, the welds create rigid connections between all members, raising questions about whether the structure remains truly reciprocal or belongs to the category of gridshell structures.
- Fig. 11(b): The rigid bolted connection (Qi et al. 2021) is designed to ensure a rigid joint between tubes, irrespective of their relative orientation. However, its bulk impacts both aesthetics and architectural expression. For modeling purposes, a rigid arm AB is fixed at point A, with only five DoFs fixed at point B. The remaining DoF is the rotation about the axis perpendicular to the plane containing the axis of the carried tube and the line AB, which is semirigid. The connection has been verified through testing on an SM RS^{3D} comprising six beams with support ends welded to a rigid frame, showing a discrepancy of less than 10% between numerical simulations and experimental measurements.
- Fig. 11(c): The bolted pinned connection (Gelez et al. 2011b) used for the RS^{2D}, presented in Fig. 1(f), is realized with a single bolt that allows rotation about its axis, while the five other DoFs are considered fixed. The authors point out that this type of connection provides a structural behavior equivalent to a hinge, under vertical loading and at first order.
- Fig. 11(d): The scaffolding swivel connector (Sénéchal et al. 2011) is a simple solution that allows rapid and economical construction of an RS^{3D}. In terms of modeling, the eccentricity can be represented by a rigid arm allowing free rotation around its axis at the pivot. Nevertheless, drawbacks include poor aesthetics and the fact that rotation of the members about their axis is only prevented by friction from tightening, making it challenging to model accurately.
- Fig. 11(e): In the fully through-bolt connection (Rizzuto and Popovic 2010), a bolt passes entirely through both tubes, with saddleback washers at the contact interfaces to better distribute stresses between the tubes. Rizzuto and Popovic (2010) model this connection in four ways: All six DoFs are restrained, while in the others, a hinge is introduced either at one end of the eccentricity or at its midpoint. The authors observe that the first modeling approach correlates better with experimental results than the others. Subsequently, Rizzuto (2018) used the same connection for a larger RS^{3D}, modeling the connection with six semirigid DoFs, as shown in Fig. 8(a). The stiffnesses were determined from a local model where 2D shell elements modeled the tubes and bolt. However, experimental validation could not be achieved due to horizontal movements of the supports [Fig. 5(b)], which modified the tested geometry and disrupted displacement measurements during testing.
- Fig. 11(f): The partially through-bolt connection (Steinmetz et al. 2024) is an alternative to the previous solution. It aims to simplify the connection behavior and reduce the number of fixed DoFs. The connection can be modeled by a hinge positioned at the tube interface (point B), linked to the tube axes by rigid arms (AB and BC). The modeling results and experimental displacement measurements [for a simple RS^{3D} with three beams, as shown in Fig. 5(d)] differ by an average of 5.5%. However, stress measurements show a mean discrepancy of 15.3%, as the rotational DoFs between the tubes are slightly semirigid due to contact between the bolt head and the supported tube at point B.
- Fig. 11(g): The ball-based connection (Steinmetz et al. 2024) is proposed by the authors as another alternative solution to release rotational DoFs completely. A ball is placed inside the supported tube, allowing free rotation relative to the ball's center, with an

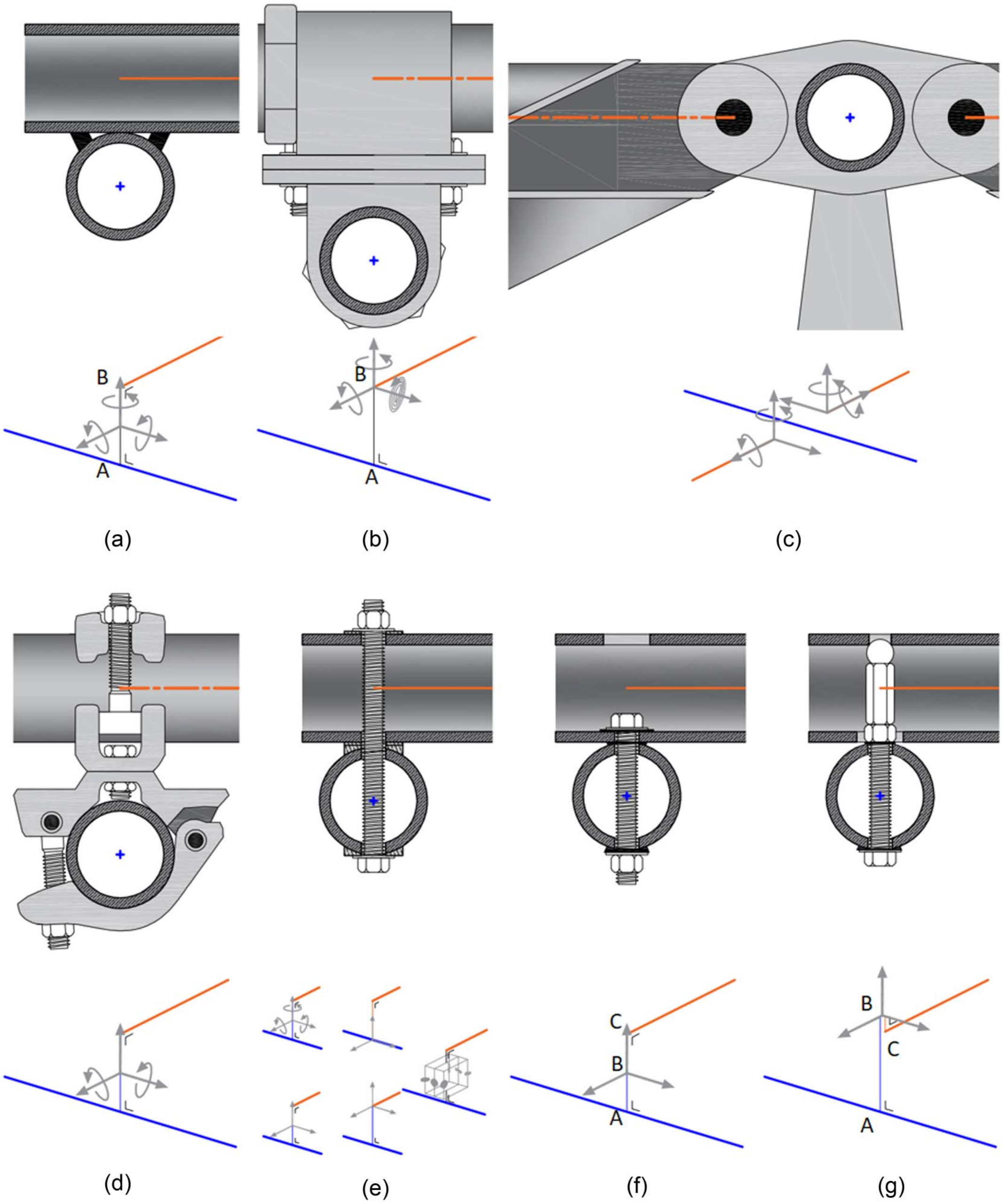

Fig. 11. (a) Welded connection; (b) rigid bolted connection; (c) bolted pined connection; (d) scaffolding swivel connector; (e) fully through-bolt connection; (f) partially through-bolt connection; and (g) ball-based connection.

opening made in the carried tube at the midpoint of the eccentricity. The model then consists of a perfect hinge at the ball's center, connected to the tube axes via a short beam AB, which accounts for the fastener properties, and a rigid arm BC. Modeling results show displacements and stress magnitudes within 5% of experimental measurements on a simple RS^{3D} geometrically identical to that shown in Fig. 5(d). However, this assembly only functions if the ball remains in contact with the supported tube, thus limiting its applicability.

Discussion on Semirigid DoF in Connections and Supports

As explained in this section, the supports and connections often exhibit specific semirigid DoFs due to friction, clearances, machining tolerances, lever arms between bolts, and other factors. Such semirigidities are often unavoidable; however, the authors recommend minimizing them as far as possible for the following three main reasons:

- They affect the transmission of forces between beams and may cause localized plastic deformations or failures that are difficult to predict.
- In principle, they should be modeled as semirigid DoFs, but their behavior is often nonlinear and extremely difficult to evaluate. Nonetheless, neglecting them in numerical models leads to overestimating deflections and internal forces within the beams, which is safe at the structural level, though not necessarily at the local level.
- Finally, the greater the number of restrained DoFs in the connections, the more the structure departs from an actual reciprocal

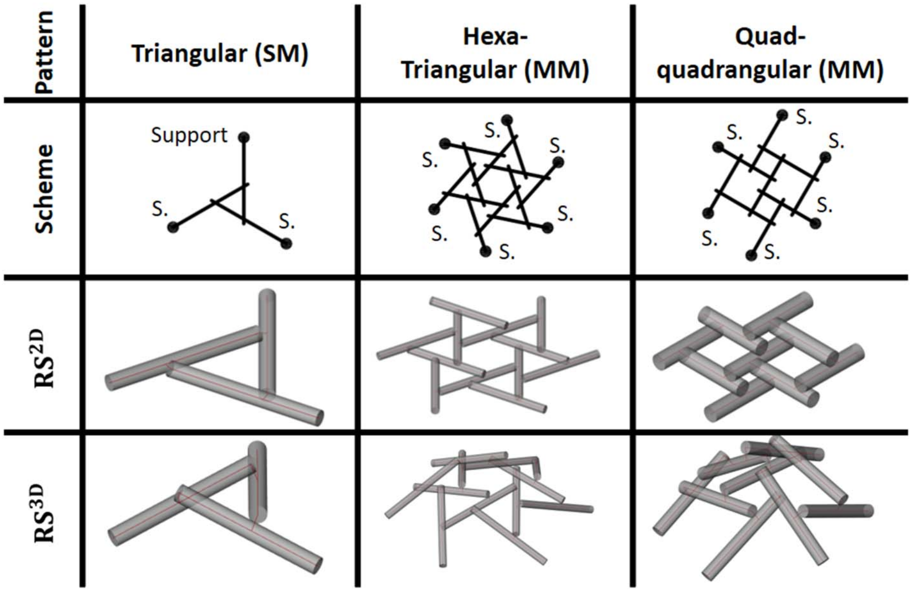

Fig. 12. Varying RS^{2D} and RS^{3D} with their pattern and diagram. Supports (S.) are indicated with circles.

structure and approaches the behavior of a gridshell. Although gridshells have advantages, this shift results in the loss of the distinctive architectural character of reciprocal structures and the potential for modular construction, where elements can be stacked to span large distances with small components.

Nevertheless, the fewer the fixed DoFs, the lower the local or global stability is assured. Consequently, the following sections of this paper are dedicated to methods for verifying local and global stability.

Existing Approaches for RS Geometric Stability Assessment

This section presents and compares the effectiveness of five methods that can be employed to verify the stability of an RS.

Geometric instability must be distinguished from elastic instability.

- Geometric instability is a mechanism with one or more "rigid movements." A rigid movement refers to a beam's movement that is independent of any elastic deformation due to internal forces. Geometrically unstable structures are called "kinematically indeterminate."
- Elastic instability occurs when excessive force creates the buckling of either a single beam or the whole structure. It depends on the geometry of the structure, the mechanical and cross-sectional properties of the beams, and the loading.

This paper only focuses on geometric instability and compares four methods, respectively, developed by Gelez et al. (2011a), Brocato (2011), Xia et al. (2019), and Wackerfuß (2020). In this article, they will be referred to as follows:

- Method 1: Local Stability Method (LSM)
- Method 2: Kinematic Analysis Method (KAM)
- Method 3: Kinematic Compatibility Matrix Analysis Method (KCMAM)
- Method 4: Constraint Matrix Analysis Method (CMAM)

In addition, a Method 0, the well-known classical finite element method, will serve as a benchmark to validate the results of the four previous methods, given that it considers the mechanical and cross-sectional properties of the beams, and therefore distinguishes itself from the other four methods.

These methods are compared based on the patterns illustrated in Fig. 12. Unless stated otherwise, the modeling assumptions for the supports and connections are based on those presented in Fig. 4.

Method 0: Stiffness Matrix Analysis Method

Method 0 determines the stability of a structure by analyzing the eigenvalues λ of its stiffness matrix $\mathbf{K}$. These eigenvalues are computed by solving $\mathbf{K}\mathbf{v} = \lambda\mathbf{v}$, where $\mathbf{v}$ is an eigenvector of the stiffness matrix. A null value of at least one eigenvalue implies a mechanism, which is described by its corresponding eigenvector (Kannan et al. 2014). This analysis, which we shall refer to as the stiffness matrix analysis method (SMAM), applies to both RS^{2D} and RS^{3D}, regardless of the fixed DoFs at the supports and connections. However, this analysis is computationally expensive and requires defining the beam's material and cross-sectional properties.

Method 1: Local Stability Method

The LSM consists of analyzing the global stability of an RS^{2D} or RS^{3D} based on the local stability of each beam. The method is founded on the principle that if the six possible movements of each beam are restrained, considering only the fixed DoFs at its ends (at connections and/or supports), then the structure is deemed stable (Gelez et al. 2011a). This method, for example, confirms the stability of the RS^{2D} presented in Fig. 13(a) (Gelez et al. 2011a). Indeed, each beam is locally stable when considering only the fixed DoFs at its end: On one side, three translational DoFs (T_x, T_y, and T_z) are fixed, and on the other side, two translational DoFs (T_y and T_z) and one rotational DoF (R_x) are fixed.

Applying the same principle to the RSs shown in Figs. 13(b and c) would lead to the conclusion that both structures are unstable, which is incorrect in the case of Fig. 13(c). Although each beam has three fixed translational DoFs at each end, they can still rotate around their longitudinal axis (R_x). While the structure in Fig. 13(b) is indeed unstable, the RS^{3D} of Fig. 13(c) is, in fact, stable, as can be demonstrated using other methods discussed in this paper. This discrepancy is explained by the fact that the LSM neglects the stabilization that the supported beams may provide.

J. Struct. Eng., 2026, 152(3): 04025288

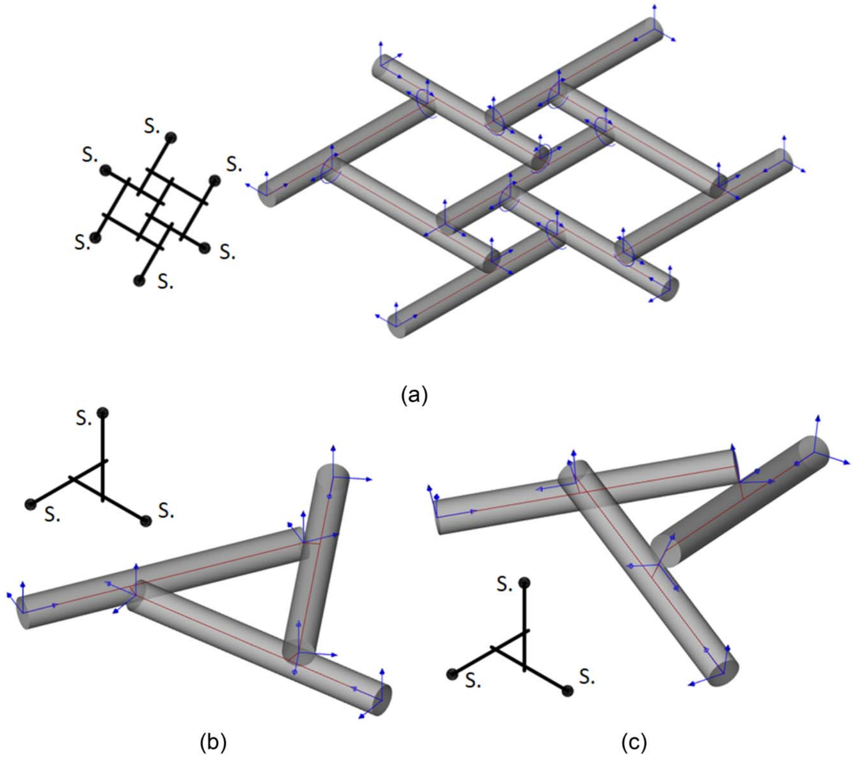

Fig. 13. RSs with their diagram and a perspective view with arrows indicating the fixed DoFs at connection and supports: (a) stable RS^{2D}; (b) unstable RS^{2D}; and (c) stable RS^{3D}.

The drawback of this method is that it may classify specific structures as unstable when, in fact, they are stable. In other words, this method can guarantee that an RS is stable but not that it is unstable. It has the advantage of being simple, quick to implement, and conservative, but it may unnecessarily limit the designer's choice of structural solutions.

Method 2: Kinematic Analysis Method

Through a vector analysis, this method enables the determination of rigid body movements between beams in an RS^{3D}, considering only the fixed DoFs at the connections. Based on the number of these rigid movements, it is possible to determine the minimum number of DoFs that must be fixed at the supports to make the RS stable. The connection between beams is assumed to be identical throughout and is based on the following assumptions [Fig. 14(a)] (Brocato 2011):

- It is a variant of Fig. 4(c), where the supporting beam is considered to have no thickness (the eccentricity AB is fully embedded within the supported beam).
- In addition to fixing the three translational DoFs, the connection also prevents the rotation about the y-axis R_y, passing through the connection point A [Fig. 14(a)]. Thus, each connection allows two relative rotations between two beams: one about the eccentricity axis AB and the other about the axis of the supporting beam.

Based on these assumptions and without considering the fixed DoFs at the supports, Brocato (2011) stated that an MM RS^{3D} composed of n_{int} connections and f single modules exhibits $2 \cdot n_{int} - 5 \cdot f$ rigid body movements of beams. To guarantee the global stability of the RS, the author concludes that the number of fixed DoFs that must be provided at the supports should be greater than or equal to $2 \cdot n_{int} - 5 \cdot f + 6$.

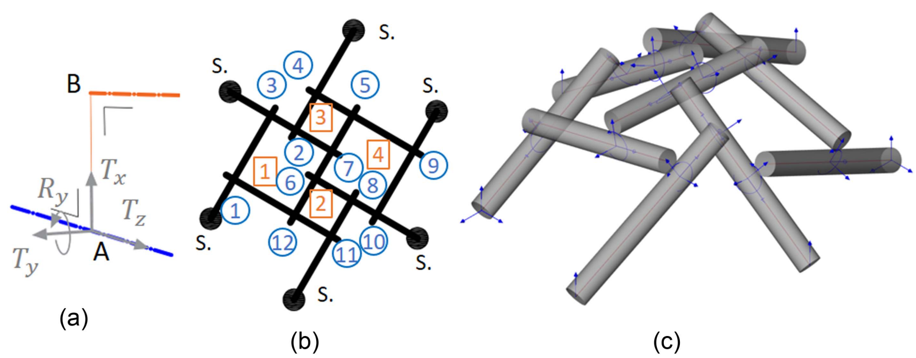

Fig. 14. (a) RS^{3D} connection type considered by this method; (b) RS^{3D} with $n_{int} = 12$ connections (circled numbers) and $f = 4$ single modules (framed numbers); and (c) perspective view with arrows indicating the fixed DoFs at connections.

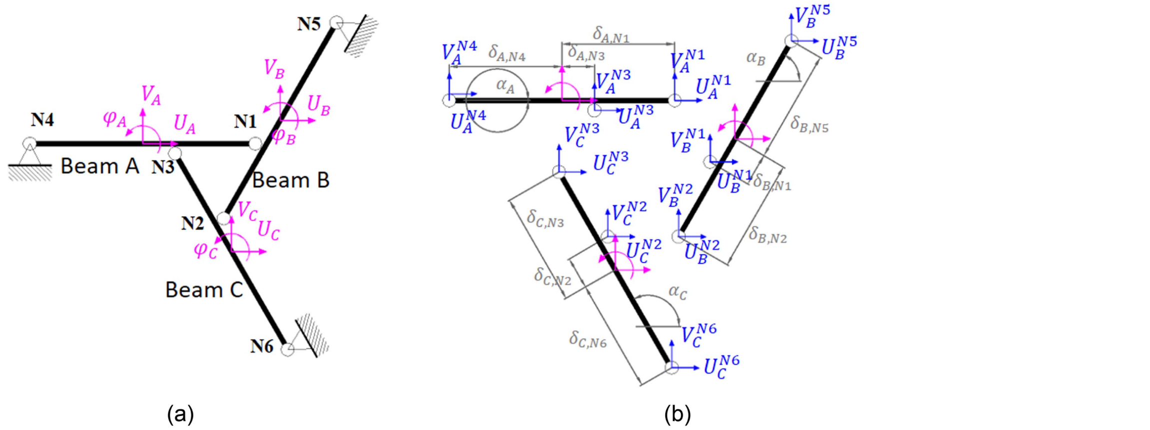

Fig. 15. (a) RS^{1D} with three beams (A, B, and C), each having three rigid body movements (U, V, and φ); and (b) RS decomposed to express the bonded movements fixed at the supports and between the beams.

Brocato (2011) illustrated this formula with the MM RS^{3D} shown in Fig. 14(b) ($n_{int} = 12$, $f = 4$), for which it is necessary to provide $2 \cdot n_{int} - 5 \cdot f + 6 = 2.12 - 5.4 + 6 = 10$ support reactions distributed among the six support points. The author suggests, for example, using two hinged supports and four roller supports, blocking only the vertical direction.

This method allows for a rapid and straightforward determination of the number of DoFs that must be fixed at the supports to ensure the stability of an RS. However, it is limited to a unique type of connection, assuming a null thickness for the supporting beam. The author has not extended the method to RS^{2D}, for which different connection assumptions would be required.

Method 3: Kinematic Compatibility Matrix Analysis Method

The KCMAM was developed by Parigi et al. (2014) for RS^{1D} structures with hinged connections. Subsequently, Xia et al. (2019) extended it to RS^{2D} and RS^{3D} structures. The Parigi et al. (2014) method is illustrated for an RS^{1D} composed of three beams in Fig. 15(a), each possessing three rigid body displacements (U, V, and φ) indicated at their center of gravity. An RS^{1D} is a special case of RS^{2D} where both the external loading and the structure are defined within the same plane. Fig. 15(b) shows the fixed movements at each beam's support and connection nodes. These fixed movements at the supports and connections can be expressed as the following kinematic compatibility equations between the restrained movements:

- At the supports: $U_A^{N4} = V_A^{N4} = U_B^{N5} = V_B^{N5} = U_C^{N6} = V_C^{N5} = 0$
- At the connections: $U_A^{N1} = U_B^{N1}$, $V_A^{N1} = V_B^{N1}$, $U_B^{N2} = U_C^{N2}$, $V_B^{N2} = V_C^{N2}$, $U_A^{N3} = U_C^{N3}$, and $V_A^{N3} = V_C^{N3}$.

These node movements are then expressed in terms of the rigid body movements of the beams. For example, at connection node N1, $U_A^{N1} = U_B^{N1}$ becomes $U_A - \delta_B^{N1} \sin(\alpha_A)\, \varphi_A = U_B - \delta_B^{N1} \sin(\alpha_B) \varphi_B$. Finally, the system can be written in the following matrix form: $\mathbf{B}\ \mathbf{d} = 0$ where $\mathbf{B}$ is the kinematic compatibility matrix and $\mathbf{d}$ is the vector of rigid body movements of the beams.

For a structure with b beams, if r is the rank of matrix $\mathbf{B}$, the number of mechanisms is given by $n_k = 3b - r$ and the structure is thus unstable if $n_k > 0$. The RS shown in Fig. 15 presents no mechanisms ($n_k \leq 0$).

Xia et al. (2019) extended the method to 3D space, applying it to RS^{2D} and RS^{3D} structures with fully hinged supports and connections (RS_{Hinged}), respectively located at the end of the centroidal axis and at the half eccentricity, as shown in Fig. 4. In three dimensions, calculating the number of mechanisms becomes $n_k = 6b - r$ to account for the three additional rigid body displacements.

These authors analyzed the stability of RS_{Hinged}^{2D} and RS_{Hinged}^{3D} structures, with triangular and hexatriangular patterns (Fig. 16). The two RS^{2D} structures were declared unstable with, respectively, 3 and 12 instability modes. In contrast, the RS^{3D} structures were found to be stable. Despite these interesting results, the method developed by Xia et al. (2019) applies only to RS with fully hinged assemblies and supports. However, accounting for fixed rotational DoF appears possible.

Method 4: Constraint Matrix Analysis Method

The CMAM was developed by Wackerfuß (2019, 2020) in a general context, without having been applied explicitly to RS. This section summarizes the method and examines how it can be advantageously applied to RS.

The method is illustrated in Fig. 17 using an unstable plane structure composed of two bars connected by a hinge and supported on two pinned supports. The bars connect nodes $N1$ to $N2$ and $N3$ to $N4$. A fictitious element of zero length represents the hinge, linking nodes $N2$ and $N3$, which are in fact coincident. Each node has two translational DoFs expressed in the (x, y) coordinate system.

The following three types of constraints are considered, which can be expressed in matrix form in Eq. (1):

- Invariability of bar length: $\Delta L^{N1,N2} = U_1 - U_3 = 0$ and $\Delta L^{N3,N4} = U_5 - U_7 = 0$ (rows 1 and 2).
- Fixed displacements at the supports: $U_1 = U_2 = U_7 = U_8 = 0$ (rows 3 to 6).
- Connection conditions: $U_3 = U_5$ and $U_4 = U_6$ (rows 7 and 8)

$$\begin{bmatrix} 1 & 0 & -1 & 0 & 0 & 0 & 0 & 0 \\ 0 & 0 & 0 & 0 & 1 & 0 & -1 & 0 \\ 1 & 0 & 0 & 0 & 0 & 0 & 0 & 0 \\ 0 & 1 & 0 & 0 & 0 & 0 & 0 & 0 \\ 0 & 0 & 0 & 0 & 0 & 0 & 1 & 0 \\ 0 & 0 & 0 & 0 & 0 & 0 & 0 & 1 \\ 0 & 0 & 1 & 0 & -1 & 0 & 0 & 0 \\ 0 & 0 & 0 & 1 & 0 & -1 & 0 & 0 \end{bmatrix} \begin{bmatrix} U_1 \\ U_2 \\ U_3 \\ U_4 \\ U_5 \\ U_6 \\ U_7 \\ U_8 \end{bmatrix} = \begin{bmatrix} 0 \\ 0 \\ 0 \\ 0 \\ 0 \\ 0 \\ 0 \\ 0 \end{bmatrix} \quad (1)$$

The matrix is then reduced to triangular form through Gaussian elimination, to identify the number of nonzero rows,

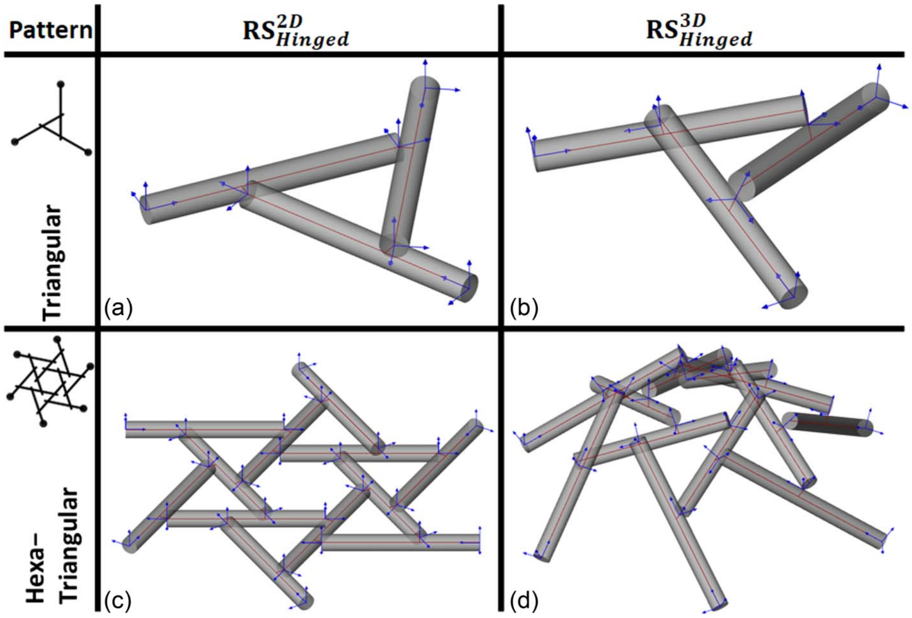

Fig. 16. RS with triangular and hexatriangular patterns, hinged supports, and connections: (a) unstable $n_k = 3$; (b) stable; (c) unstable $n_k = 12$; and (d) stable.

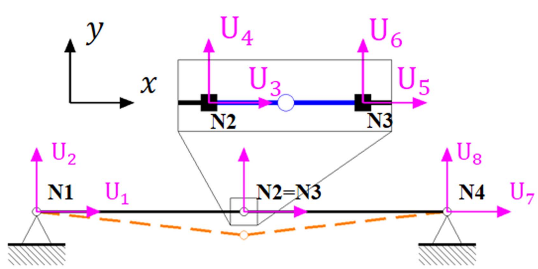

Fig. 17. Illustration of the constraint matrix analysis method with an example of a two-bar unstable structure.

corresponding to the matrix rank r. It should be noted that this operation may rearrange the matrix rows and change the order of DoFs in the vector in Eq. (2)

$$\begin{bmatrix} 1 & 0 & -1 & 0 & 0 & 0 & 0 & 0 \\ 0 & 1 & 0 & -1 & 0 & 0 & 0 & 0 \\ 0 & 0 & 1 & 0 & 0 & 0 & 0 & 0 \\ 0 & 0 & 0 & 1 & 0 & 0 & 0 & 0 \\ 0 & 0 & 0 & 0 & 1 & 0 & 0 & 0 \\ 0 & 0 & 0 & 0 & 0 & 1 & 0 & 0 \\ 0 & 0 & 0 & 0 & 0 & 0 & 1 & -1 \\ 0 & 0 & 0 & 0 & 0 & 0 & 0 & 0 \end{bmatrix} \begin{bmatrix} U_1 \\ U_5 \\ U_3 \\ U_7 \\ U_2 \\ U_8 \\ U_4 \\ U_6 \end{bmatrix} = \begin{bmatrix} 0 \\ 0 \\ 0 \\ 0 \\ 0 \\ 0 \\ 0 \\ 0 \end{bmatrix} \qquad (2)$$

Based on the matrix rank r (number of nonzero rows, here $r = 7$) and the total number n of DoFs (number of columns, here $n = 8$), the number of mechanisms can be calculated as $n_k = n - r$, which is 1 in the case of the structure in Fig. 17. The corresponding instability mode, shown as a dotted line in Fig. 17, can be obtained as follows:

1. Complete the matrix by inserting a 1 in the diagonal element of the zero row (in this case, imposing $U_6 = 1$). If $n_k > 1$, a 1 is successively placed in each zero row's diagonal elements to compute each instability mode.
2. Solve the system to compute the other displacements, which provides a displacement vector representing the instability mode.

The general matrix form can be written as $\mathbf{C}_{m\times n}\ \mathbf{u}_n = 0_m$, where the constraint matrix C contains the m constraints (rows), and $\mathbf{u}$ is the vector of n DoFs (columns). The matrix $\mathbf{C}$ is thus not necessarily square, and it is a necessary (but not sufficient) condition for stability that $m \geq n$.

To generalize this method to RS^{2D} and RS^{3D}, certain aspects illustrated in Fig. 18 must be specified, as follows:

- The method defines two types of rigid elements: wire and meshed. A wire element is modeled as a bar connecting two nodes, as in the example of Fig. 17. A meshed element is modeled as a rigid polygon decomposed into triangles (flat meshed element) for planar cases, or as a rigid polyhedron decomposed into tetrahedra (space meshed element) for spatial cases.
- Structural elements, supports, and joints each have their local reference frame. It is therefore necessary to transform constraints from the local to the global coordinate system, in which DoFs are expressed. Fig. 18 shows the local reference systems for different structural elements. The local frame of a wire element is defined by its axis (x^{loc}) and another chosen direction. The local frame of a meshed element is defined by three nodes forming a triangle.
- The spatial movement of meshed elements can be fully defined by the three translational DoFs of the nodes forming the element. In contrast, for wire elements, an additional rotational DoF about x^{loc} must be added to account for the possibility of axial rotation. Specifically, for RSs, their beams can be modeled as wire elements representing their median fibers, but this also implies modeling many wire elements to represent the eccentricities between the beam axes (Fig. 18). This drawback, combined with the need to introduce a rotational DoF per wire element, suggests that using flat meshed elements for RS^{2D} and flat or space meshed elements for RS^{3D}, depending on the beam type (Fig. 2), is a more suitable approach.

Comparison of Methods

The four methods previously presented, along with the Method 0 (SMAM), were tested on three RS^{2D} and three RS^{3D} structures,

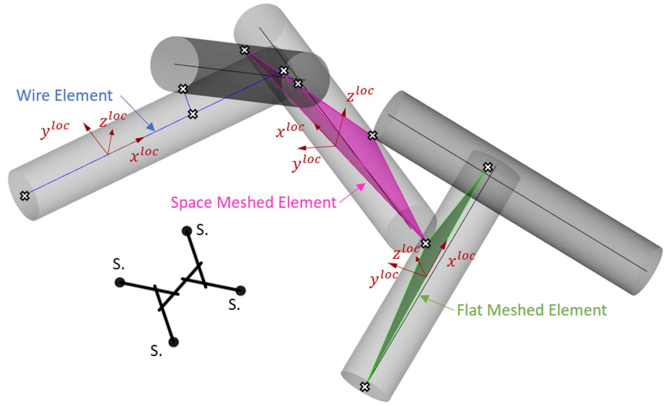

Fig. 18. Modeling of RS beams using wire, flat meshed, and space meshed elements, with their respective local coordinate system.

labelled a, b, c, d, e, and f, as illustrated in Fig. 19. As a reminder, "hinged" refers to structures where all supports and joints are hinged (i.e., R_x, R_y, and R_z are free).

Fig. 20 summarizes the results obtained and provides the size of the analyzed matrices.

- The SMAM applies to all RS configurations but requires a significantly larger matrix analysis than the other matrix-based methods. It also requires defining the material and cross-section properties of the beams. To ensure that the stiffness matrix is minimally affected by these modeling choices, it is necessary to impose artificially high stiffness properties to isolate instability modes related solely to the geometry and configuration of blocked or free DoFs.
- The LSM is a universal method that guarantees RS stability. However, it classifies some structures as unstable, which are, in fact, stable; thereby, it considerably restricts the designer's freedom. Although all three RS^{3D} structures analyzed are labelled as unstable by the LSM, they are stable.
- The KAM and KCMAM methods provide a correct assessment of RS stability but are not universally applicable in their current developments; they are limited to specific configurations of fixed DoFs at supports or joints and/or to certain RS types.
- For RS_{Hinged}, KCMAM and CMAM (with meshed elements) produce matrices of identical dimensions.
- CMAM correctly determines the stability of RS structures and is the only method, based on the assumption of infinitely rigid beams, that can be applied unconditionally to all RS^{2D} and RS^{3D} types, regardless of the assumptions made regarding supports and connections.

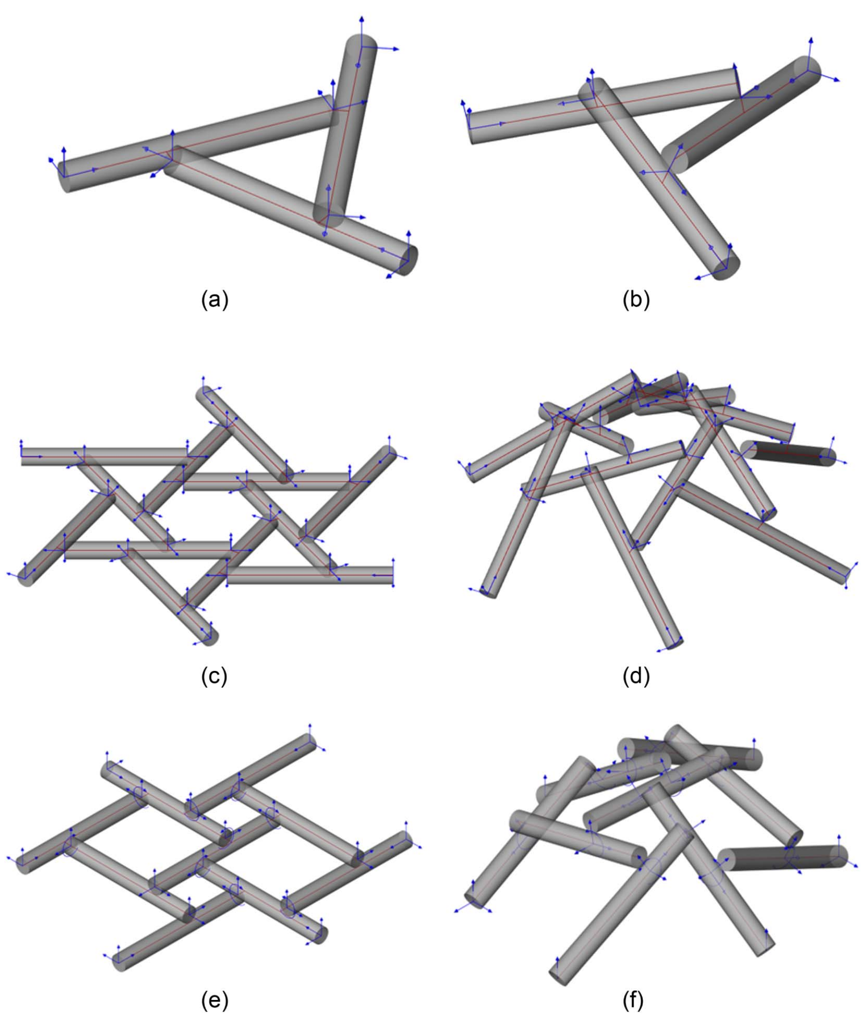

Fig. 19. Geometry of the six RSs studied in the table of Fig. 20: (a) SM RS^{2D}_{Hinged} triangular (unstable); (b) MM RS^{2D}_{Hinged} hexa-triangular (unstable); (c) MM RS^{2D} quad-quadrangular (stable); (d) SM RS^{3D}_{Hinged} triangular (stable); (e) MM RS^{3D}_{Hinged} hexa-triangular (stable); and (f) MM RS^{3D} quad-quadrangular (stable).

J. Struct. Eng., 2026, 152(3): 04025288

Structure			Stable?	Hinged?	Methods				
Type	N°	Patt.			0) SMAM	1) LSM	2) KAM	3) KCMAM	4) CMAM
RS^{2D}	a		No	Yes	n_k=3 [54 × 54]	Unstable	ND	n_k=3* [18 × 18]	n_k=3 [18 × 18]
	b		No	Yes	n_k=12 [252 × 252]	Unstable	ND	n_k=12* [72 × 72]	n_k=12 [72 × 72]
	c	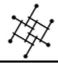	Yes	No	Stable [180 × 180]	Stable*	ND	ND	Stable [90 × 90]
RS^{3D}	d	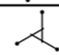	Yes	Yes	Stable [72 × 72]	Unstable	ND	Stable* [18 × 18]	Stable [18 × 18]
	e		Yes	Yes	Stable [360 × 360]	Unstable	ND	Stable* [72 × 72]	Stable [72 × 72]
	f		Yes	No	Stable [240 × 240]	Unstable	Stable*	ND	Stable [94 × 90]

Fig. 20. Summary of the results obtained using the five methods on six different structures. Matrix sizes are indicated in each case. Asterisks (*) denote results obtained from the cited references; the authors of this paper produced the others. ND = Not developed by the authors or not applicable.

This comparison demonstrates that CMAM, although not initially developed for RS applications, is the only method, under the assumption of rigid beams, that allows for stability verification across all RS types, independently of the hypotheses made on supports and connections. It also enables the identification of potential instability modes and their corresponding geometric configurations. However, by adding the possibility of fixing rotational DoF in the KCMAM, the latter would be as applicable and valuable as the CMAM.

Discussion

Special Case of RS_{Hinged}

Previously, we discussed the semirigid DoFs that can exist in particular supports and connections, and which we recommend limiting as much as possible through sound and thoughtful design. If all DoFs are rigidly fixed (e.g., by welding the steel beams together), the structure no longer strictly qualifies as an RS but becomes a gridshell. While gridshells are of interest, they depart from the definition of RS, which relies instead on the "stacking" of hinged-connected beams. The RS_{Hinged} represents a special case of RS in which all supports and connections allow complete rotational freedom about all three axes. These structures are always statically determinate: For a configuration with b beams and $n_{tot} = 2b$ nodes (support or connection), the total number of fixed DoFs at the nodes is $3n_{tot}$, which equals the total number of rigid body motions ($6b = 3n_{tot}$).

The authors recommend using RS_{Hinged} whenever possible, as they offer the following two significant advantages:

- They are statically determinate and thus easier to assemble. In statically indeterminate RSs, improper placement of one beam can make it impossible to place the subsequent one(s) (Goto et al. 2011).
- Supports and connections are identical at every node, simplifying their fabrication.

The RS^{2D}_{Hinged} structures A and B from Fig. 19, whose instability modes are shown in Figs. 21(a and b), are unstable because their beams can freely rotate about their longitudinal axis. To ensure stability, it is necessary to block this axial rotation for each beam, either at the connections or at the supports. In contrast, the RS^{3D}_{Hinged} shown in Figs. 19(d and e) are stable, as the presence of supported beams prevents axial rotation of the supporting beams. Unlike RS^{2D} configurations, the beam axes in RS^{3D} are not coplanar but are offset by an eccentricity that acts as a lever arm capable of resisting rotation.

However, certain RS^{3D}_{Hinged} structures can still be unstable, as illustrated by the RS in Figs. 21(c and d). In these cases, the instability arises from a rotational movement of the central beam around its longitudinal axis, which induces motion in the other beams. This instability mode tends to appear in RS^{3D}_{Hinged} with symmetrical patterns featuring a central symmetry axis through the center of a beam, such as the bitriangular and quad-quadrangular patterns.

It is important to note that all four RSs illustrated in Fig. 21 are stable in their displaced configurations (i.e., under second-order effects and after large displacements), as is the case for the structure in Fig. 17. Xia et al. (2019) demonstrated this for the two RS^{2D}_{Hinged} of Figs. 21(a and b). For the two RS^{3D}_{Hinged} cases [Figs. 21(c and d)], the displacement of the beams inevitably breaks the central symmetry, thereby rendering them second-order stable in their deformed configuration.

Conclusions are summarized below.

- RS^{2D}_{Hinged} structures are always unstable, regardless of the pattern. It is necessary to design connections and/or supports that block axial rotation of the beams, at least at one of their ends.
- RS^{3D}_{Hinged} structures are often stable, except for particular geometries that exhibit a central axis of symmetry passing through the center of a beam. If necessary in some cases, fixing the supports can be a simple and effective solution for transforming an unstable RS^{3D}_{Hinged} into a stable RS^{3D}_{Hinged}.

Accuracy and Efficiency of KCMAM and CMAM

Stability verification for the KCMAM and CMAM methods relies on the rank of the kinematic compatibility matrix **B** and the constraint matrix **C**. Studies in the literature (Pellegrino 1993; Wackerfuß 2020; Xia et al. 2019) recommend computing the rank using singular value decomposition (SVD), a more robust algebraic method than Gaussian elimination. Compared to the latter, an SVD of a matrix is more numerically stable (less impacted by rounding effects or inaccuracies in the positioning of nodes) and provides more insight than just its rank.

An SVD decomposes a matrix $\mathbf{A}_{k\times l}$ into two orthogonal matrices ($\mathbf{P}_{k\times k}$ and $\mathbf{D}_{l\times l}$), and a diagonal matrix $\boldsymbol{S}_{k\times l}$ containing the "singular values" s_i (all nonnegative) and all nondiagonal entries being zero. This results in the factorization: $\mathbf{A} = \mathbf{PSD^T}$. The singular values are arranged in descending order: $s_{\max} \geq \ldots \geq s_i \geq \ldots \geq s_{\min} \geq 0$. It should be noted that, when the matrix **A** is square and symmetric,

J. Struct. Eng., 2026, 152(3): 04025288

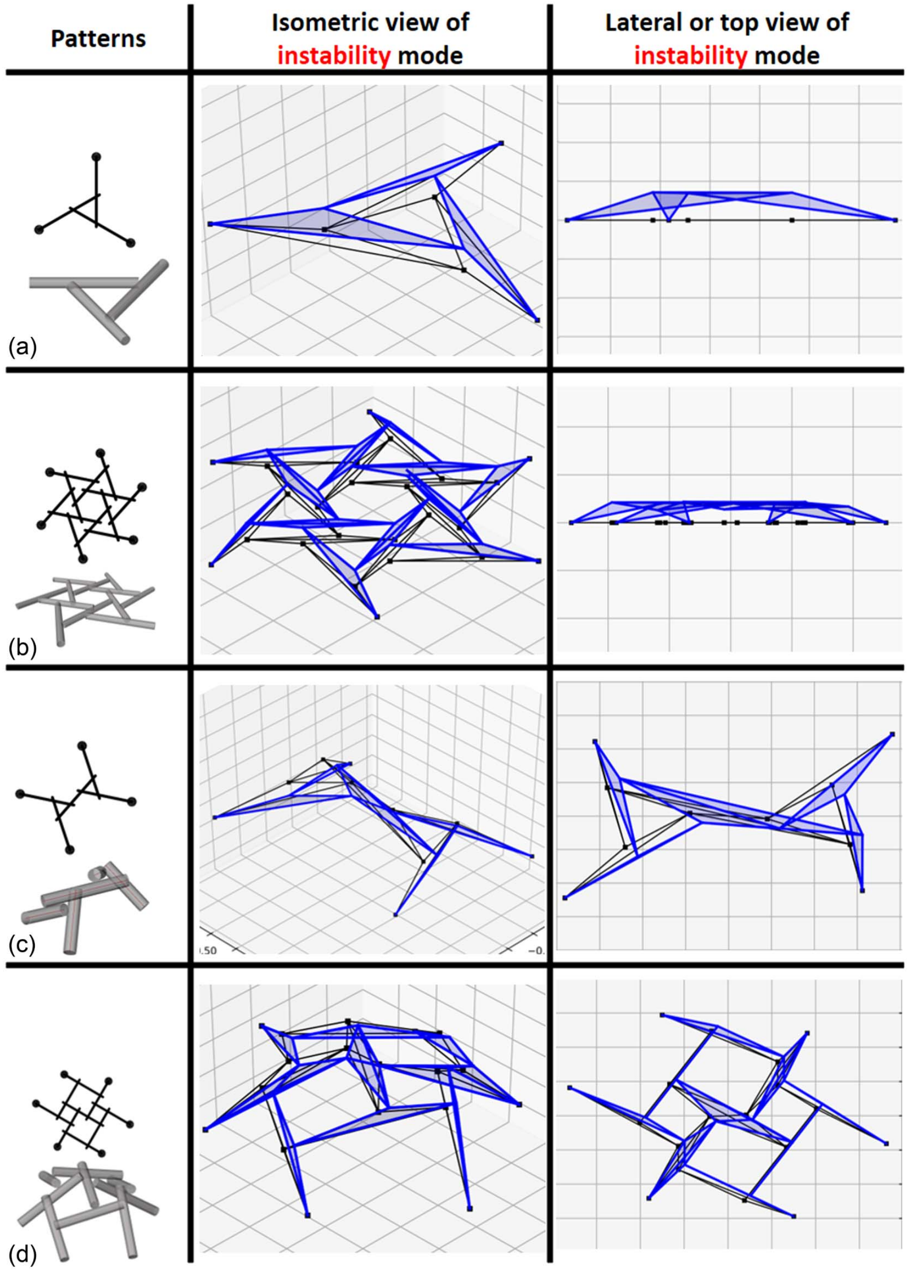

Fig. 21. Instability modes of various $\mathrm{RS}^{2D}_{\mathrm{Hinged}}$: (a) triangular; and (b) hexa-triangular; and $\mathrm{RS}^{3D}_{\mathrm{Hinged}}$: (c) bi-triangular; and (d) quad-quadrangular.

its singular values coincide with its eigenvalues. If $\mathbf{A}$ is singular, at least its smallest singular value ($s_{\min}$) will be exactly or numerically zero.

Based on the singular values of $\mathbf{A}$, a "condition number" $\kappa = s_{\max}/s_{\min} \in [1; \infty]$ can be defined (Trefethen and David 1997). According to Trefethen and David (1997), the matrix $\mathbf{A}$ is considered well-conditioned if κ is small ($\kappa \leq 10^3$) and ill-conditioned if κ is large ($\kappa \geq 10^6$).

These algebraic tools allow a qualitative assessment of the stability of an RS based on the condition number κ of the constraint or kinematic compatibility matrix. A small κ value indicates that the RS is likely to be stable, whereas a large value suggests instability.

Fig. 22 provides the values of $s_{\min}$, $s_{\max}$, and κ for the constraint matrix (CMAM) associated with four $\mathrm{RS}^{3D}_{\mathrm{Hinged}}$ structures modeled using either wire elements or meshed elements, whose stability was previously discussed. The values of $s_{\min}$, $s_{\max}$, and κ vary little between the two modeling approaches. Moreover, the κ values reveal an order-of-magnitude difference of approximately 10^{14} between stable and unstable RSs. The two stable structures have a condition number below 10^3, supporting the validity of the criterion above.

Fig. 23 illustrates the variation in the condition number κ for the unstable structures of Fig. 22 and the beam of Fig. 17, when their geometries are slightly modified.

For the beam of Fig. 23(a), the condition number κ decreases rapidly with even a slight change of the angle α. suggesting that the structure is stable ($\kappa = 10^3$) for $\alpha = \pm 0.19°$. However, depending on the cross-sectional area of the beam, the displacement of the central node can be high and must be checked by Method 0 because $\alpha = 0.19°$ is a very small angle.

As for Fig. 23(b), the geometry of the bitriangular or quad-quadrangular $\mathrm{RS}^{3D}_{\mathrm{Hinged}}$ is slightly nonsymmetrically modified by

RS^{3D}_{HINGED}	Wire Elements			Meshed Elements		
	s_{min} (-)	s_{max} (-)	κ (-)	s_{min} (-)	s_{max}(-)	κ (-)
Triangular: STABLE	0.063	6.70	106	0.078	2.11	27
Hexa-triangular: STABLE	0.028	5.26	188	0.026	3.06	119
Bi-triangular: UNSTABLE	8.21×10^{-16}	9.56	116×10^{14}	1.93×10^{-16}	3.02	157×10^{14}
Quad-quadrangular: UNSTABLE	8.48×10^{-16}	8.56	101×10^{14}	9.07×10^{-16}	3.03	33×10^{14}

Fig. 22. Values of $s_{\min}$, $s_{\max}$, and κ for four RS^{3D}_{Hinged} modeled with wire elements or meshed elements.

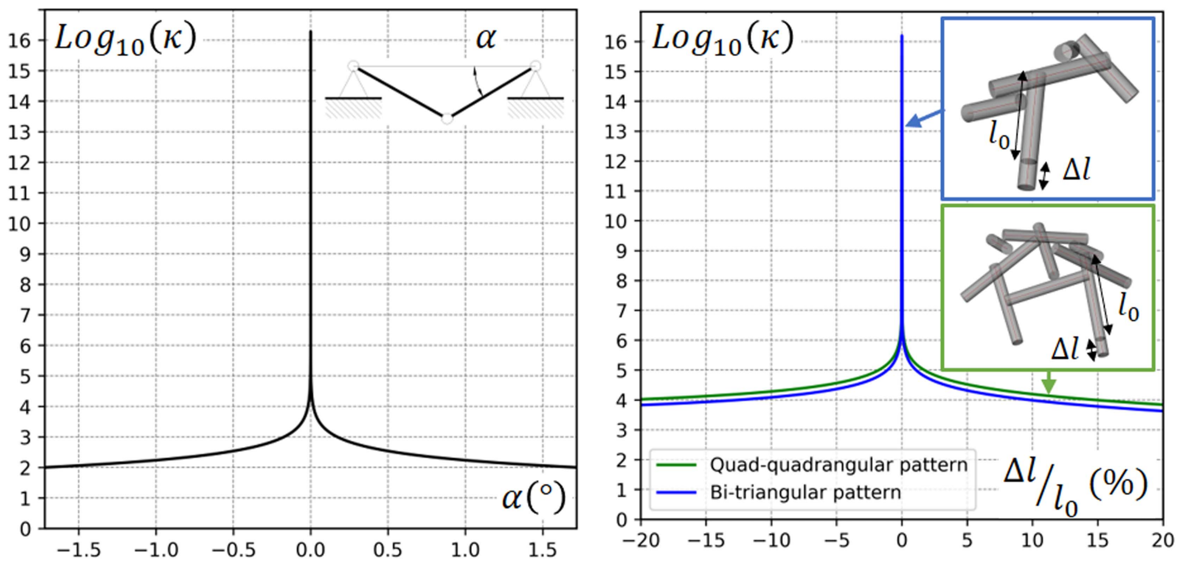

(a) (b)

Fig. 23. κ values (logarithmic scale) for structures with geometric variation: (a) central hinged beam; and (b) bitriangular and quad-quadrangular patterns.

increasing the length of one support beam. After such a modification, these structures are no longer symmetric and are therefore considered stable when computing the rank after Gaussian elimination. However, the condition number falls within a moderate range (between 10^3 and 10^6), which requires a complete stability calculation using method 0.

Fig. 24(a), related to the simple unstable double beam, gives the values of the middle node displacement for a specific case with several values of α.

Fig. 24(b), related to the stable hexatriangular RS in Fig. 22, provides the value of the maximum nodal displacement for a specific case, which is limited to 2.4 mm, confirming the good stability of the structure and its low displacements.

Figs. 24(c and d), related to the unstable bitriangular and quad-quadrangular RS of Fig. 22, modified with a relative elongation of 20% of the support beam, provide the values of the maximum nodal displacement, respectively 55 and 363 mm, which can be considered excessive.

The structures of Figs. 24(b and c) have identical cross sections, materials, total loads, eccentricities, and similar spans.

These examples show that the qualitative discussion on the structure's stability, based on κ, needs to be confirmed by a comprehensive structural analysis. Additionally, the proposed threshold at 10^3 does not ensure limited displacements for reasonable cross sections.

Conclusion

Five methods for verifying the stability of RSs have been studied and compared. Except for Method 0, these methods assume that the beams are infinitely rigid, enabling the determination of RS geometric stability at a preliminary design stage without assigning cross-sections. Indeed, unstable RSs need to be rejected, as they would never satisfy the building codes, or would require an excessive amount of materials.

Table 1 summarizes the advantages and disadvantages of each, demonstrating that CMAM is the most effective and universal, as it applies to all types of RSs regardless of the DoF fixed at supports and connections. In addition, this method enables a qualitative discussion of RS stability based on the condition number κ, thereby expanding the scope of rejected unstable RSs.

These methods have shown that certain RS_{Hinged} can be geometrically stable under specific conditions. For RS^{2D}_{Hinged}, rotational DoFs about the longitudinal axis of each beam must be blocked either at the connections or at the supports. In contrast, most

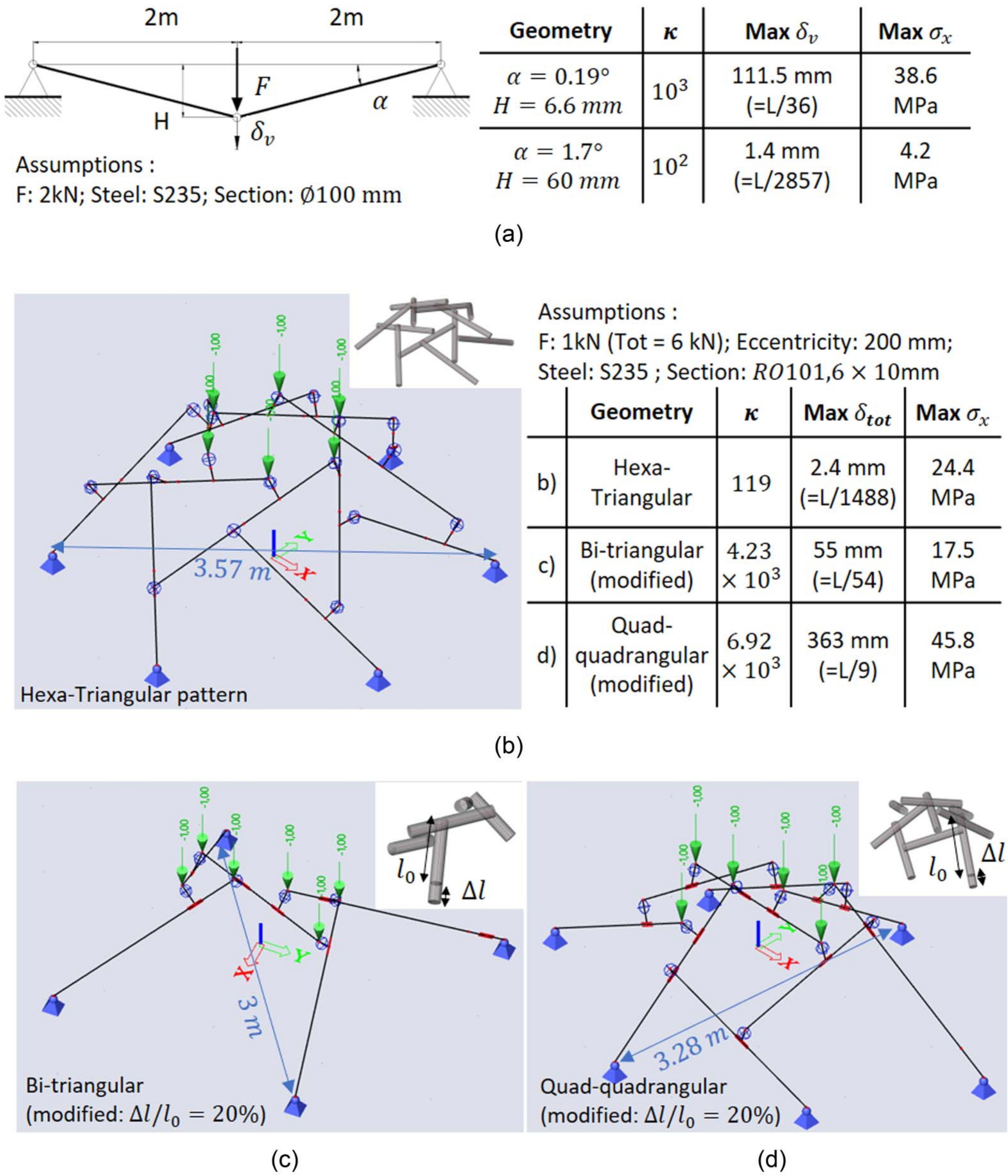

Fig. 24. Structural analysis of structures using SCIA engineering software: (a) central hinged beam; (b) stable hexatriangular pattern; (c) unstable bitriangular pattern (modified); and (d) unstable quad-quadrangular pattern (modified).

Table 1. Advantages and disadvantages of RS's five stability verification methods

Method		Considered structures			
No.	Name	Blocked DoF	RS type	Advantages	Disadvantages
0	SMAM	Arbitrary	RS^{2D} and RS^{3D}	Applicable to all RSs	Computationally demanding; requires complete numerical modeling and definition of all material and cross-section properties
1	LSM	Arbitrary	RS^{2D} and RS^{3D}	Intuitive and fast; no matrix calculations	Identifies some stable structures as unstable
2	KAM	Imposed	RS^{3D}	Simple formula, no matrix computations	Not yet developed for all RSs
3	KCMAM	Imposed	RS^{2D} and RS^{3D}	Reduces the matrix size to be analyzed	Not yet developed for all RSs
4	CMAM	Arbitrary	RS^{2D} and RS^{3D}	Universally applicable to all RSs	

RS^{3D}_{Hinged} are geometrically stable, as this axial rotation is inherently prevented due to the eccentricity between the supporting and supported beams, which creates a stabilising lever arm. Finally, RS^{3D}_{Hinged} are geometrically unstable if they exhibit central symmetry through the center of a beam. If necessary, in some cases, fixing the supports can be a simple and effective solution for transforming an unstable RS^{3D}_{Hinged} into a stable RS^{3D}_{Hinged}.

Furthermore, an examination of the supports and connections used in existing RSs, whether in laboratory specimens, scaled prototypes, or full-scale structures, reveals the following:

J. Struct. Eng., 2026, 152(3): 04025288

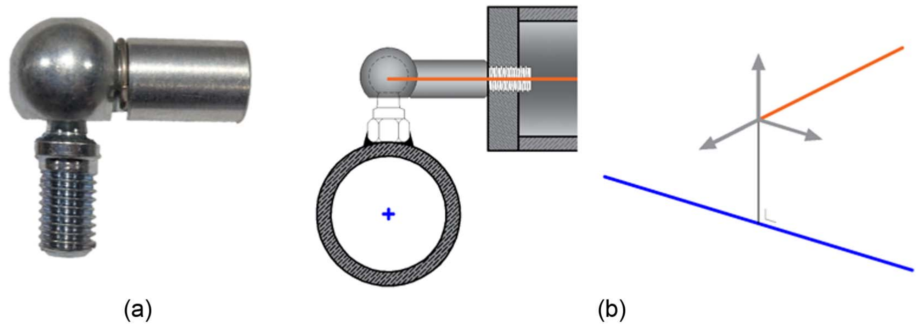

Fig. 25. Proposal for a hinge connection using a ball and socket joint: (a) picture of a commercial joint; and (b) diagram and model when using the joint in a $\mathrm{RS}^{\mathrm{3D}}_{\mathrm{Hinged}}$.

- Designers often opt to fix an excessive number of DoFs, leading to increased stiffness but at the expense of ease of assembly and a behavior closer to that of gridshells.
- Supports and connections often exhibit semirigid DoFs, which should be avoided in practice. These arise from friction, machining tolerances, or assembly gaps, and are challenging to model accurately, despite their significant influence on overall structural behavior.
- The design and modeling of supports play a critical role in ensuring the structural stability of RSs. Nevertheless, this is not a widely studied topic.

The authors therefore recommend favoring $\mathrm{RS}_{\mathrm{Hinged}}$ using hinged supports and connections, and where necessary, blocking axial rotation at least at one end of each beam or fixing the supports. However, no connection in the literature offers a truly hinged behavior for connections, as they invariably exhibit some degree of semirigidity. For metallic $\mathrm{RS}^{\mathrm{3D}}$, the authors propose using commercial ball-and-socket joints, as illustrated in Fig. 25(a), which allow a hinged connection between two metal tubes [Fig. 25(b)].

Data Availability Statement

All data, models, or code generated or used during the study are available from the corresponding author by request.

Author Contributions

Martin Steinmetz: Conceptualization; Formal analysis; Investigation; Methodology; Validation; Visualization; Writing – original draft. Luca Sgambi: Conceptualization; Investigation; Resources; Supervision; Writing – original draft; Writing – review and editing. Pierre Latteur: Conceptualization; Investigation; Resources; Supervision; Writing – original draft; Writing – review and editing.

Notation

The following symbols are used in this paper:

B = kinematic compatibility matrix;
b = number of beams of an RS;
C = constraints matrix;
f = number of single modules of a multiple module reciprocal structure;
K = stiffness matrix of a structure;
n_{int}, n_{tot} = number of connections (int) or supports and connections (tot) of a reciprocal structure;
n_k = number of mechanisms in a structure;
R_x, R_y, R_z = rotational degrees of freedom of a support or connection;
r = rank of matrix;
s_i, $s_{\min}$, $s_{\max}$ = singular value of a matrix, minimal and maximal;
T_x, T_y, T_z = translational degrees of freedom of a support or connection;
U, V, φ and $\boldsymbol{d}$ = translational and rotational rigid movements of a beam in the kinematic compatibility matrix analysis method, and the vector regrouping them;
U_i and $\mathbf{u}$ = global translational DoF of nodes in the constraint matrix analysis method, and the vector regrouping them;
$\mathbf{v}$ = eigenvector of a stiffness matrix;
x^{loc}, y^{loc}, z^{loc} = local coordinate system of element in the constraint matrix analysis method;
κ = condition number; and
λ = eigenvalue of a stiffness matrix.

References

Anastas, Y., L. Rhode-Barbarigos, and S. Adriaenssens. 2016. "Design-to-construction workflow for cell-based pattern reciprocal free-form structures." *J. Int. Assoc. Shell Spatial Struct.* 57 (2): 159–176. https://doi.org/10.20898/j.iass.2016.188.737.

Baverel, O. 2000. *Nexorades: A family of interwoven space structures*, 1–323. Guildford, UK: Univ. of Surrey.

Bergis, L., and K. D. Rycke. 2019. "Reciprocal frame for the roof of the Franz Masereel Centre." In Vol. 2017 of *Proc. of Int. Association for Shell and Spatial Structures Annual Symp.*, No. 7, 1–10. Madrid, Spain: International Association for Shell and Spatial Structures.

Brocato, M. 2011. "Reciprocal frames: Kinematical determinacy and limit analysis." *Int. J. Space Struct.* 26 (4): 343–358. https://doi.org/10.1260/0266-3511.26.4.343.

Castriotto, C., F. Tavares, G. Celani, O. Popovic Larsen, and X. Browne. 2022. "Clamp links: A novel type of reciprocal frame connection." *Int. J. Archit. Comput.* 20 (2): 378–399. https://doi.org/10.1177/14780771211054169.

Corio, E., F. Laccone, N. Pietroni, P. Cignoni, and M. Froli. 2017. "Conception and parametric design workflow for a timber large-spanned reversible grid shell to shelter the archaeological site of the roman shipwrecks in Pisa." *Int. J. Comput. Methods Exp. Meas.* 5 (4): 551–561. https://doi.org/10.2495/CMEM-V5-N4-551-561.

Descamps, T., and G. Guerlement. 2009. "Component method for the assessment of the axial, shear and rotational stiffness of connections in old timber frames." In *Proc., 9ème Congrès National de Mécanique*. Casablanca, Morocco: Societé Marocaine Des Sciences Mécaniques.

Douthe, C., and O. Baverel. 2009. “Design of nexorades or reciprocal frame systems with the dynamic relaxation method.” *Comput. Struct.* 87 (21–22): 1296–1307. https://doi.org/10.1016/j.compstruc.2009.06.011.

Franke, L., A. Stahr, C. Dijoux, and C. Heidenreich. 2017. “How does the zollinger node really work? A structural experimental investigation to a better understanding of the nodal behavior.” In Vol. 2017 of *Proc., Int. Association for Shell and Spatial Structures Annual Symp.*, No. 11, 1–10. Madrid, Spain: International Association for Shell and Spatial Structures.

Garavaglia1a, E., A. Pizzigoni2b, and L. Sgambi. 2013. “Collapse behaviour in reciprocal frame structures.” *Struct. Eng. Mech.* 46 (4): 533–547. https://doi.org/10.12989/sem.2013.46.4.533.

Gelez, S., S. Aubry, and B. Vaudeville. 2011a. “Behavior of a simple nexorade or reciprocal frame system.” *Int. J. Space Struct.* 26 (4): 331–342. https://doi.org/10.1260/0266-3511.26.4.331.

Gelez, S., S. Aubry, and B. Vaudeville. 2011b. “Nexorade or reciprocal frame system applied to the design and construction of a 850 M2 archaeological shelter.” *Int. J. Space Struct.* 26 (4): 303–311. https://doi.org/10.1260/0266-3511.26.4.303.

Geno, J., J. Goosse, S. Van Nimwegen, and P. Latteur. 2022. “Parametric design and robotic fabrication of whole timber reciprocal structures.” *Autom. Constr.* 138 (Apr): 104198. https://doi.org/10.1016/j.autcon.2022.104198.

Godina Rodriguez, M. C. 2019. “Design framework for bamboo culms—A study of bamboo reciprocal structures.” Ph.D. thesis, Univ. College London. https://discovery.ucl.ac.uk/id/eprint/10080507/.

Goto, K., R. Kidokoro, and T. Matsuo. 2011. “Rokko mountain observatory.” *Arup J.* 46 (2): 20–26.

Gustafsson, J. 2016. “Connections in timber reciprocal frames.” Master’s thesis, Dept. of Civil and Environmental Engineering, Chalmers Univ. of Technology.

Kannan, R., S. Hendry, N. J. Higham, and F. Tisseur. 2014. “Detecting the causes of ill-conditioning in structural finite element models.” *Comput. Struct.* 133 (Mar): 79–89. https://doi.org/10.1016/j.compstruc.2013.11.014.

Kohlhammer, T., A. A. Apolinarska, F. Gramazio, and M. Kohler. 2017. “Design and structural analysis of complex timber structures with glued T-joint connections for robotic assembly.” *Int. J. Space Struct.* 32 (3–4): 199–215. https://doi.org/10.1177/0266351117746268.

Larsen, O. P. 2008. *Reciprocal frame architecture*. Abingdon, UK: Routledge.

Larsson, M., H. Yoshida, and T. Igarashi. 2019. “Human-in-the-loop fabrication of 3D surfaces with natural tree branches.” In *Proc., 3rd Annual ACM Symp. on Computational Fabrication*, 1–12. New York: Association for Computing Machinery. https://doi.org/10.1145/3328939.3329000.

Latteur, P., J. Geno, and M. Vandamme. 2021. “Design rules for timber log reciprocal floors, based on mass optimization under stiffness constraint.” *Int. J. Space Struct.* 36 (3): 217–240. https://doi.org/10.1177/09560599211041699.

Nguyen, A. C., P. Vestartas, and Y. Weinand. 2019. “Design framework for the structural analysis of free-form timber plate structures using wood-wood connections.” *Autom. Constr.* 107 (Aug): 102948. https://doi.org/10.1016/j.autcon.2019.102948.

Parigi, D., and P. H. Kirkegaard. 2014a. “Design and fabrication of free-form reciprocal structures.” *Nexus Network J.* 16 (1): 69–87. https://doi.org/10.1007/s00004-014-0177-9.

Parigi, D., and P. H. Kirkegaard. 2014b. “The reciprocalizer: An agile design tool for reciprocal structures.” *Nexus Network J.* 16 (1): 61–68. https://doi.org/10.1007/s00004-014-0176-x.

Parigi, D., M. Sassone, P. H. Kirkegaard, and P. Napoli. 2014. “Static and kinematic formulation of planar reciprocal assemblies.” *Nexus Network J.* 16 (1): 37–59. https://doi.org/10.1007/s00004-014-0175-y.

Pellegrino, S. 1993. “Structural computations with the singular value decomposition of the equilibrium matrix.” *Int. J. Solids Struct.* 30 (21): 3025–3035. https://doi.org/10.1016/0020-7683(93)90210-X.

Pizzigoni, A. 2009. “A high fiber reinforced concrete prototype for reciprocal structures of demountable building a high fiber reinforced concrete prototype for reciprocal structures of demountable building.” In *Proc., Symp. Int. Association for Shell and Spatial Structures (50th. 2009. Valencia). Evolution and Trends in Design, Analysis and Construction of Shell and Spatial Structures: Proc*. Valencia, Spain: Universitat Politècnica de València.

Popovic Larsen, O. 2014. “Reciprocal frame (RF) structures: Real and exploratory.” *Nexus Network J.* 16 (1): 119–134. https://doi.org/10.1007/s00004-014-0181-0.

Qi, L., Z. Li, H. Pan, L. Li, and X. Huang. 2021. “Study on adjustable connector of reciprocal frame.” *Stavební Obzor—Civ. Eng. J.* 30 (2): 378–392. https://doi.org/10.14311/cej.2021.02.0028.

Rizzuto, J. P. 2018. “Experimental investigation of reciprocally supported element (RSE) lattice honeycomb domes structural behaviour.” *Eng. Struct.* 166 (Feb): 496–510. https://doi.org/10.1016/j.engstruct.2018.03.094.

Rizzuto, J. P., and O. L. Popovic. 2010. “Connection systems in reciprocal frames and mutually supported elements space structure networks.” *Int. J. Space Struct.* 25 (4): 243–256. https://doi.org/10.1260/0266-3511.25.4.243.

Sénéchal, B., C. Douthe, and O. Baverel. 2011. “Analytical investigations on elementary nexorades.” *Int. J. Space Struct.* 26 (4): 313–320. https://doi.org/10.1260/0266-3511.26.4.313.

Song, P., C. W. Fu, P. Goswami, J. Zheng, N. J. Mitra, and D. Cohen-Or. 2013. “Reciprocal frame structures made easy.” *ACM Trans. Graph.* 32 (4): 1–13. https://doi.org/10.1145/2461912.2461915.

Steinmetz, M., P. Latteur, and L. Sgambi. 2023. “Optimal log floor patterns.” *Eng. Struct.* 297 (Jun): 116970. https://doi.org/10.1016/j.engstruct.2023.116970.

Steinmetz, M., L. Sgambi, and P. Latteur. 2024. “Reliable experimental testing methodology for reciprocal structures.” In *Proc., IASS Annual Symp.*, 1–10. Madrid, Spain: International Association for Shell and Spatial Structures.

Trefethen, L. N., and B. David. 1997. *Numerical linear algebra*. Philadelphia: Society for Industrial and Applied Mathematics.

Vestartas, P., A. Rezaei Rad, and Y. Weinand. 2021. “Robotically-fabricated nexorades from whole timber.” In *Proc., Int. fib Symp. on Conceptual Design of Structures*, edited by C. Fivet, P. D'Acunto, M. Fernández Ruiz, and P. O. Ohlbrock, 539–546. Madrid, Spain: Institute for Construction Science.

Wackerfuß, J. 2019. “On the detection, visualization and characterization of spurious kinematic modes in arbitrary plane structures.” *Int. J. Solids Struct.* 164 (Jun): 84–103. https://doi.org/10.1016/j.ijsolstr.2018.12.023.

Wackerfuß, J. 2020. “A direct numerical method to evaluate the geometric stability of arbitrary spatial structures.” *Int. J. Solids Struct.* 185 (Mar): 29–45. https://doi.org/10.1016/j.ijsolstr.2019.10.027.

Wrench, T. 2015. *A simple roundhouse manual*. Scotts Valley, CA: CreateSpace Independent Publishing Platform.

Xia, Y. Q., N. Xiao, H. P. Chen, and X. Q. Qian. 2019. “Determination of static and kinematic determinacy of pin-jointed assemblies using rigid-body displacements as primary unknown variables.” *Eng. Struct.* 181 (Jun): 643–652. https://doi.org/10.1016/j.engstruct.2018.12.037.